JOURNAL OF NATURAL PRODUCTS

pubs.acs.org/jnp

Article

Leveraging Peptaibol Biosynthetic Promiscuity for Next-Generation Antiplasmodial Therapeutics

Jin Woo Lee,[§] Jennifer E. Collins,[§] Karen L. Wendt, Debopam Chakrabarti,* and Robert H. Cichewicz*

Cite This: *J. Nat. Prod.* 2021, 84, 503−517

Read Online

ACCESS | Metrics & More | Article Recommendations | Supporting Information

ABSTRACT: Malaria remains a worldwide threat, afflicting over 200 million people each year. The emergence of drug resistance against existing therapeutics threatens to destabilize global efforts aimed at controlling *Plasmodium* spp. parasites, which is expected to leave vast portions of humanity unprotected against the disease. To address this need, systematic testing of a fungal natural product extract library assembled through the University of Oklahoma Citizen Science Soil Collection Program has generated an initial set of bioactive extracts that exhibit potent antiplasmodial activity (EC_{50} < 0.30 μg/mL) and low levels of toxicity against human cells (less than 50% reduction in HepG2 growth at 25 μg/mL). Analysis of the two top-performing extracts from *Trichoderma* sp. and *Hypocrea* sp. isolates revealed both contained chemically diverse assemblages of putative peptaibol-like compounds that were responsible for their antiplasmodial actions. Purification and structure determination efforts yielded 30 new peptaibols and lipopeptaibols (**1**−**14** and **28**−**43**), along with 22 known metabolites (**15**−**27** and **44**−**52**). While several compounds displayed promising activity profiles, one of the new metabolites, harzianin NPDG I (**14**), stood out from the others due to its noteworthy potency (EC_{50} = 0.10 μM against multi-drug-resistant *P. falciparum* line Dd2) and absence of gross toxicity toward HepG2 at the highest concentrations tested (HepG2 EC_{50} > 25 μM, selectivity index > 250). The unique chemodiversity afforded by these fungal isolates serves to unlock new opportunities for translating peptaibols into a bioactive scaffold worthy of further development.

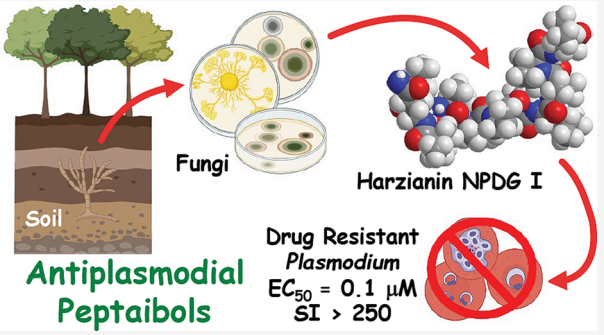

Malaria is a devastating infectious disease caused by *Plasmodium* spp. parasites, transmitted through the bite of female *Anopheles* spp. mosquitoes. This disease is prevalent throughout tropical and sub-Saharan regions, with pregnant women and children facing the highest risk of mortality. Despite recent improvements afforded by artemisinin combination therapy (ACT), malaria remains a major health and economic burden to developing countries, with 229 million cases reported in 2019 alone.[1] Approved treatments for malaria consist of several chemical scaffolds including (i) sesquiterpene peroxides (e.g., artemisinin derivatives and analogues), (ii) quinoline ring derivates (e.g., quinine, quinidine, primaquine, mefloquine, atovaquone, chloroquine), (iii) antifolates (e.g., pyrimethamine, sulfadoxine), and (iv) repurposed antibiotics (e.g., clindamycin, doxycycline, tetracycline) (Figure 1). Notably, this group of therapeutics is dominated by natural products, which have been a mainstay of antimalarial agents for many decades. Unfortunately, growing levels of clinical resistance have been observed for all the compounds listed, and their administration is often limited due to an assortment of dose-limiting side effects.[2−4] Of particular concern is the spread of artemisinin-resistant parasites throughout large portions of the Greater Mekong Subregion in Southeast Asia.[5] This has led to a precarious healthcare situation, as monitoring efforts have revealed increasing levels of artemisinin resistance among *Plasmodium* parasites. Considering the healthcare burden imposed by malaria, emerging threats presented by the parasite, and the yet unanswered demand for safer and more effective therapeutics, there is a critical need to identify new antiplasmodial scaffolds for lead development.

The historic success achieved from applying natural products to the field of malaria treatment provides hope for future discovery efforts based on natural scaffolds. To this end, peptides are one class of natural products that offer promising indications for focused development. To date, several types of naturally occurring peptides have been tested for their antiplasmodial properties. For example, insect-derived peptides have been shown to possess inhibitory activities against the *Plasmodium* parasite,[6] including cecropins from giant silk moths that inhibit the growth of *P. falciparum*.[7,8] Other examples include scorpine and meucine-25, obtained from

Received: December 21, 2020
Published: February 10, 2021

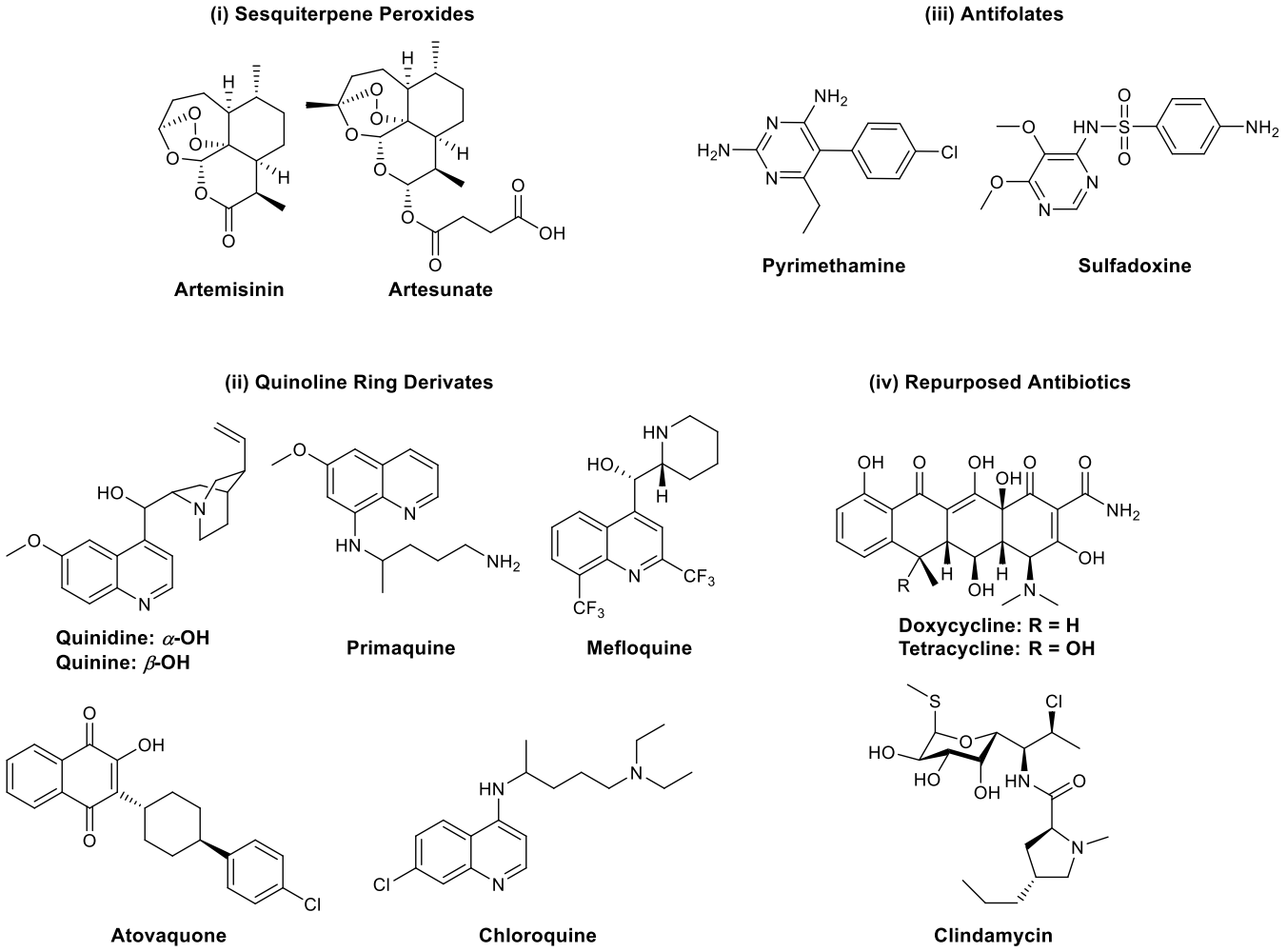

Figure 1. Structural classification of antimalarial drugs.

scorpion venom, which exhibit antimalarial effects against both *P. falciparum* and *P. berghei*.[9,10] An additional intriguing example is gambicin, which is isolated from *Anopheles* spp., and it exhibits inhibitory effects against *P. berghei* ookinetes.[11] Microorganisms represent another prospective source for the discovery of peptidic natural products with antiplasmodial activities. Gallinamide A from a marine cyanobacteria and rhabdopeptide/xenortide-like peptides from the bacterium *Xenorhabdus innexi* exhibit potent antiprotozoal activities against *P. falciparum*, with EC_{50} values of 8.4 and 0.09−3.2 μM, respectively.[12,13]

Fungi are a widely recognized source of novel peptidic molecules, but these compounds have been given scant attention as a resource for the creation of antiplasmodial leads. Among the handful of interesting antiplasmodial natural products reported from fungi are cyclic tetrapeptides such as apicidin A, which inhibits class I histone deacetylase enzymes and is lethal to *P. falciparum* with a minimum inhibitory concentration (MIC) of 0.19 μM.[14] Additionally, the kozupeptins obtained from *Paracamarosporium* sp. were shown to possess potent antiplasmodial activities against both chloroquine-sensitive and chloroquine-resistant *P. falciparum* strains, with EC_{50} values in the range of 0.15−1.46 μM.[15] Further examples of inspiring fungus-derived antiplasmodial peptidic natural products are found scattered among several groups of compounds including antiamoebin, efrapeptins, and zervamicins, which inhibit *P. falciparum* with EC_{50} values ranging from 0.45 to 6.16 μM.[16]

Recognizing the value offered by fungi and their natural products, we initiated a program to identify chemical matter that could serve as new scaffolds for antiplasmodial pharmacophore development. These efforts focused on utilizing a portion of the >66 000 isolates in the University of Oklahoma Natural Products Discovery Group screening library, which is composed primarily of fungi obtained through the Citizen Science Soil Collection Program.[17] This report focuses on our team's collaborative efforts identifying, purifying, characterizing, and testing a diverse selection of bioactive peptaibols and lipopeptaibols. These compounds provide valuable insights for the development of fungal natural products as antiplasmodial agents.

RESULTS AND DISCUSSION

An *in vitro* biological screening system was used to test over 3000 fungus-derived natural product samples from the University of Oklahoma Citizen Science Soil Collection for inhibition of the asexual stage of the intraerythrocytic life cycle of *P. falciparum*. This process included a counter screen against the HepG2 human cell line, to identify substances that afford selective toxicity against *P. falciparum*. Based on those tests, a subset of 38 extracts that exhibited potent (EC_{50} < 0.30 μg/mL) and selective (>50% growth in HepG2 at 25 μg/mL)

https://dx.doi.org/10.1021/acs.jnatprod.0c01370
J. Nat. Prod. 2021, 84, 503−517

Table 1. Inhibitory Effects of 18-AA Peptaibols (1−5 and 15−19)

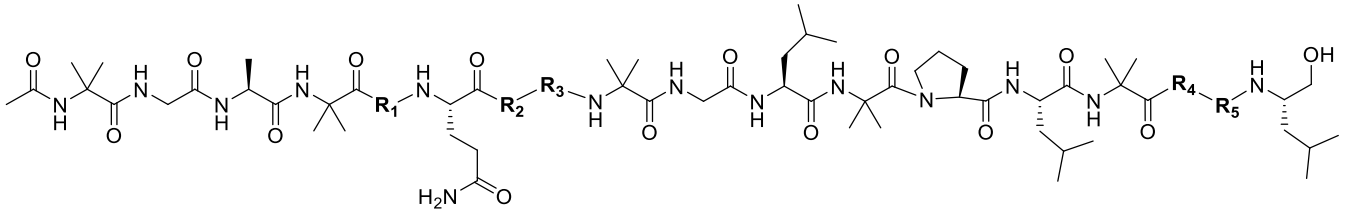

compound	MW	R_1	R_2	R_3	R_4	R_5	*P. falciparum* EC_{50} (μM)[a]	HepG2 EC_{50} (μM)[a]	selectivity index (SI)
trichorzin NPDG A (**1**)	1703	L-Ala	Aib	L-Val	D-Iva	L-Gln	1.14 ± 0.09	17.42 ± 1.70	15
trichorzin NPDG B (**2**)	1704	Aib	Aib	L-Val	Aib	L-Glu	1.66 ± 0.09	>25	>15
trichorzin NPDG C (**3**)	1731	Aib	D-Iva	L-Val	D-Iva	L-Gln	0.89 ± 0.10	12.30 ± 1.48	14
trichorzin NPDG D (**4**)	1745	D-Iva	Aib	L-Ile	D-Iva	L-Gln	0.61 ± 0.11	9.61 ± 0.63	16
trichorzin NPDG E (**5**)	1759	D-Iva	D-Iva	L-Ile	D-Iva	L-Gln	0.87 ± 0.04	6.23 ± 0.19	7
trichorzin HA I (**15**)	1703	Aib	Aib	L-Val	Aib	L-Gln	1.18 ± 0.05	21.40 ± 0.29	18
trichorzin HA II (**16**)	1717	Aib	Aib	L-Val	D-Iva	L-Gln	0.45 ± 0.06	12.80 ± 1.57	28
trichorzin HA V (**17**)	1731	D-Iva	Aib	L-Val	D-Iva	L-Gln	0.75 ± 0.09	14.67 ± 0.25	20
trichorzin HA VI (**18**)	1745	D-Iva	D-Iva	L-Val	D-Iva	L-Gln	0.92 ± 0.10	17.99 ± 0.74	20
trichorzin HA VII (**19**)	1745	D-Iva	L-Val	L-Val	D-Iva	L-Gln	0.59 ± 0.06	11.10 ± 0.92	19

[a]Results are expressed as means from triplicate experiments.

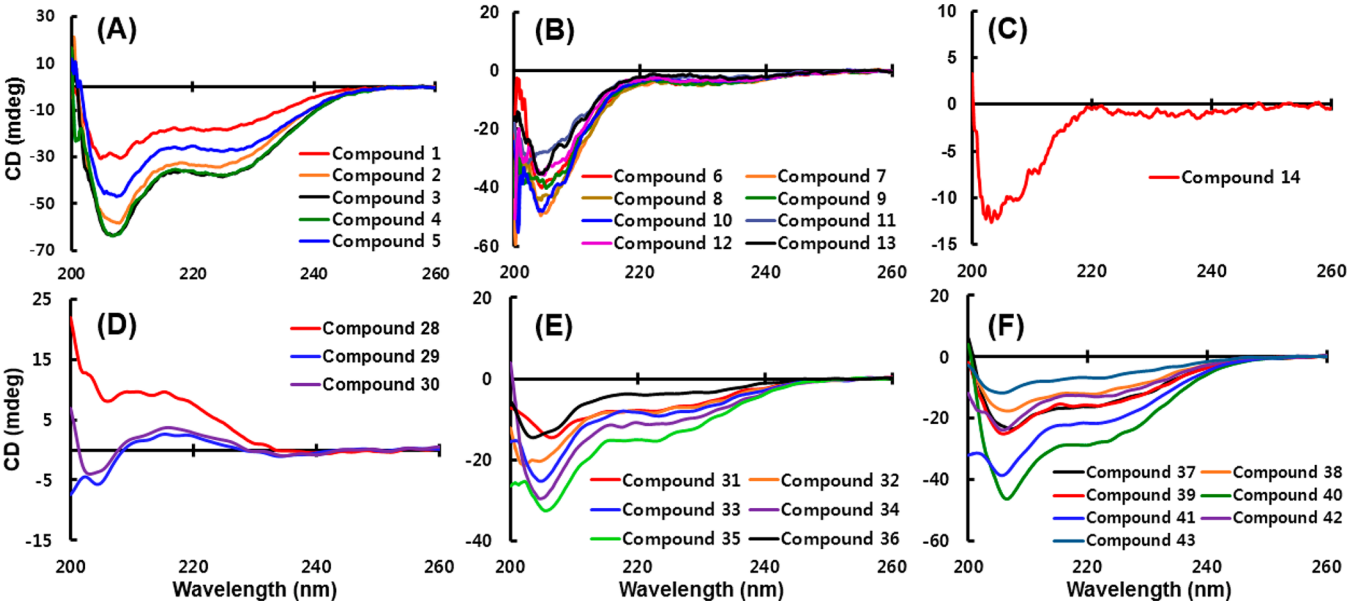

Figure 2. ECD spectra of peptaibols and lipopeptaibols: (A) peptaibols composed of 18 amino acid residues (**1**−**5**); (B) peptaibols composed of 14 amino acid residues (**6**−**13**); (C) peptaibols composed of 11 amino acid residues (**14**); (D) lipopeptaibols composed of 7 amino acid residues (**28**−**30**); (E) lipopeptaibols composed of 11 amino acid residues (**31**−**36**); and (F) lipopeptaibols composed of 15 amino acid residues (**37**−**43**).

activity against *P. falciparum* were identified. The top-performing extracts were examined by LC-MS to gain an understanding of each sample's natural product profiles. Two of the samples provided evidence that peptidic natural products were the dominant types of metabolites in the extracts. The gene sequence data for the ribosomal internal transcribed spacer (ITS) regions of the fungi were analyzed by BLAST comparisons to sequences contained in GenBank with one fungal isolate identified as a probable *Trichoderma* sp. (100% match to *Trichoderma harzianum*), and the other isolate was found to be a probable *Hypocrea* sp. (99.6% match to *Hypocrea pachybasioides*). Exploratory bioassay-guided fractionation confirmed that both extracts contained combinations of known and presumptively new peptaibols and lipopeptaibols that were responsible for the observed bioactivity. We determined that the bioactive metabolites from the isolates should be examined in tandem since their respective LC-MS data indicated both fungi were prodigious producers of nonoverlapping sets of natural products. Doing so afforded the unique opportunity to comparatively test dozens of compounds in parallel. Thus, we proceeded to generate a mini-library of peptides from the two fungal isolates using a chemistry- and bioassay-guided purification processes. Those efforts afforded a set of 30 peptaibols (**1**−**14** and **28**−**43**) that could not be matched to previously described natural products, along with 22 known compounds (**15**−**27** and **44**−**52**) for testing against *P. falciparum*.

Structure Characterization of Peptaibols from *T. harzianum*. Compound **1** was obtained as a colorless solid, and its molecular formula ($C_{79}H_{138}N_{20}O_{21}$) was ascertained

https://dx.doi.org/10.1021/acs.jnatprod.0c01370
J. Nat. Prod. 2021, 84, 503−517

from the HRESIMS data. The ^{1}H NMR spectrum of **1** contained signals representing both amide protons (δ_H 7 to 10 ppm) and α-protons derived from amino acid residues (δ_H 4 to 5 ppm), while the ^{13}C, HSQC, and HMBC NMR spectra of **1** exhibited 79 carbon signals including 20 amide carbonyls (Figure S1, Supporting Information). The HSQC, HMBC, and COSY spectrum of **1** led to the tentative identification of several structural features consistent with other *Trichoderma*-derived peptaibol natural products.[18−23] This included evidence for 18 amino acid residues consisting of a combination of 10 proteogenic amino acids [two alanines (Ala), two glycines (Gly), two leucines (Leu), two glutamines (Gln), valine (Val), and proline (Pro)] and eight non-proteogenic amino acids that are frequently associated with fungal NRPS chemistry [six α-aminoisobutyric acids (Aib), isovaline (Iva), and leucinol (Leuol)]. Analysis of the NMR data revealed additional features of prototypical peptaibol chemistry, including C-terminal (reduction of Leu to a Leuol residue) and N-terminal (acetylated Aib residue) modifications. The linear sequence of peptaibol **1** (Ac-Aib^{1}-Gly^{2}-Ala^{3}-Aib^{4}-Ala^{5}-Gln^{6}-Aib^{7}-Val^{8}-Aib^{9}-Gly^{10}-Leu^{11}-Aib^{12}-Pro^{13}-Leu^{14}-Aib^{15}-Iva^{16}-Gln^{17}-Leuol^{18}) was determined by HMBC correlations between amide carbons and amide protons, as well as ROESY correlations between α-protons. The sequence of **1** was further confirmed by interpretation of ESIMS/MS fragmentation data, which revealed the metabolite was structurally similar to trichorzin HA I (**15**) from *T. harzianum*.[24,25] A comparison of the structures of metabolites **1** and **15** revealed that **1** contained both Ala^{5} and Iva^{16} residues, whereas those positions were occupied by Aib residues in **15**. The inclusion of the Ala^{5} residue in **1** is an unusual structural feature compared to other trichorzin peptaibols (Table 1). The absolute configurations of the amino acids bearing stereogenic centers were analyzed using Marfey's method,[26,27] which revealed that amino acid residues 3, 5, 6, 8, 11, 13, 14, 17, and 18 were L-configured, whereas Iva^{16} was D-configured. The electronic circular dichroism (ECD) spectrum of **1** exhibited negative Cotton effects at 208 and 225 nm, which supported a right-handed helical conformation (Figure 2A).[28−30] Thus, the structure of peptaibol **1** was established to be Ac-Aib^{1}-Gly^{2}-L-Ala^{3}-Aib^{4}-L-Ala^{5}-L-Gln^{6}-Aib^{7}-L-Val^{8}-Aib^{9}-Gly^{10}-L-Leu^{11}-Aib^{12}-L-Pro^{13}-L-Leu^{14}-Aib^{15}-D-Iva^{16}-L-Gln^{17}-L-Leuol^{18}, and it was given the trivial name trichorzin NPDG A (**1**).

Compound **2** was obtained as a colorless solid, and its HRESIMS data were consistent with the molecular formula $C_{79}H_{137}N_{19}O_{22}$. Based on analysis of its 1D and 2D NMR, the structure of **2** was determined to be similar to that of trichorzin HA I (**15**)[24,25] with one key difference: a glutamic acid (Glu) residue replaced Gln^{17}. This conjecture was supported by analysis of the mass fragmentation data for **2**, confirming the presence and placement of Glu^{17}. The absolute configurations of the amino acids bearing stereogenic centers were confirmed by Marfey's method. Accordingly, the structure of peptaibol **2** was determined to be Ac-Aib^{1}-Gly^{2}-L-Ala^{3}-Aib^{4}-Aib^{5}-L-Gln^{6}-Aib^{7}-L-Val^{8}-Aib^{9}-Gly^{10}-L-Leu^{11}-Aib^{12}-L-Pro^{13}-L-Leu^{14}-Aib^{15}-Aib^{16}-L-Glu^{17}-L-Leuol^{18}, and it was assigned the trivial name trichorzin NPDG B (**2**). The ECD spectrum of **2** revealed negative Cotton effects at 208 and 225 nm, which indicated its right-handed helical conformation (Figure 2A).

Compound **3** was obtained as a colorless solid, and its HRESIMS data were used to assign this metabolite the molecular formula $C_{81}H_{142}N_{20}O_{21}$. The ^{13}C NMR and HMBC data for **3** provided evidence that this peptaibol contained 18 amino acid residues and was structurally similar to the reported metabolite trichorzin HA II (**16**).[24,25] The key difference between the metabolites was the Aib^{7} residue in **16** had changed to an Iva residue in **3**. This was supported by the ^{13}C NMR data, which contained two signals at δ_C 7.44 and 7.40 characteristic for the Iva γ-methyl groups. Subsequent analysis of the HMBC and ROESY, as well as MS/MS data, aided in confirming the identities and placement of each amino acid residue including both Iva residues (i.e., Iva^{7} and Iva^{16}). To confirm the absolute configurations of the chiral amino acids, Marfey's analysis was employed, thus affirming that the structure of the metabolite was Ac-Aib^{1}-Gly^{2}-L-Ala^{3}-Aib^{4}-Aib^{5}-L-Gln^{6}-D-Iva^{7}-L-Val^{8}-Aib^{9}-Gly^{10}-L-Leu^{11}-Aib^{12}-L-Pro^{13}-L-Leu^{14}-Aib^{15}-D-Iva^{16}-L-Gln^{17}-L-Leuol^{18}. This compound was assigned the trivial name trichorzin NPDG C (**3**). The ECD spectrum of **3** revealed negative Cotton effects at 208 and 225 nm, which supported its right-handed helical conformation (Figure 2A).

Upon purification, compound **4** was observed to be a colorless solid that was assigned the molecular formula $C_{82}H_{144}N_{20}O_{21}$ based on interpretation of its HRESIMS data. Analysis of the 1D and 2D NMR data for **4** revealed that its amino acid sequence was similar to that of trichorzin HA V (**17**).[24,25] One important difference noted in the ^{13}C NMR spectrum of **4** was that it contained two signals characteristic for the methyl groups of an isoleucine (δ_C16.1 and 10.8) rather than the signals attributed to a valine in **17**. Subsequent probing of the metabolite by MS/MS provided evidence supporting the sequence of **4** as Ac-Aib^{1}-Gly^{2}-Ala^{3}-Aib^{4}-Iva^{5}-Gln^{6}-Aib^{7}-Ile^{8}-Aib^{9}-Gly^{10}-Leu^{11}-Aib^{12}-Pro^{13}-Leu^{14}-Aib^{15}-Iva^{16}-Gln^{17}-Leuol^{18}. The absolute configurations of the amino acid residues were investigated using Marfey's method, which succeed in resolving most of the amino acid configurations except for the Ile residue. After several failed attempts to chromatographically resolve the products of DL-Ile and DL-*allo*-Ile by Marfey's method, a GITC (2,3,4,6-tetra-*O*-acetyl-β-D-glucopyranosyl isothiocyanate) derivatization method was used, leading to the conclusion that the metabolite contained L-Ile.[31] Thus, the structure of **4** was determined to be Ac-Aib^{1}-Gly^{2}-L-Ala^{3}-Aib^{4}-D-Iva^{5}-L-Gln^{6}-Aib^{7}-L-Ile^{8}-Aib^{9}-Gly^{10}-L-Leu^{11}-Aib^{12}-L-Pro^{13}-L-Leu^{14}-Aib^{15}-D-Iva^{16}-L-Gln^{17}-L-Leuol^{18}, and it was assigned the trivial name trichorzin NPDG D (**4**). A right-handed helical conformation was deduced for **4** based on the negative Cotton effects at 208 and 225 nm observed in its ECD spectrum (Figure 2A).

Compound **5** was purified as a colorless solid, and it was assigned the molecular formula $C_{83}H_{146}N_{20}O_{21}$ based on analysis of the HRESIMS data. The 1D and 2D NMR data for **5** indicated that the compound was a peptaibol consisting of 18 amino acid residues similar to those reported in trichorzin HA VI (**18**).[24,25] Results from the MS/MS fragmentation analysis, as well as the detection of methyl signals in the ^{13}C NMR spectrum characteristic for Ile residues (δ_C 15.9 and 10.9), led to the conclusion that the Val residue in **18** was switched to an Ile residue in **5**. To determine the absolute configurations of amino acid residues in **5**, both Marfey's and GITC methods were employed. Based on the results of those analyses, the absolute configuration of **5** was determined to be Ac-Aib^{1}-Gly^{2}-L-Ala^{3}-Aib^{4}-D-Iva^{5}-L-Gln^{6}-D-Iva^{7}-L-Ile^{8}-Aib^{9}-Gly^{10}-L-Leu^{11}-Aib^{12}-L-Pro^{13}-L-Leu^{14}-Aib^{15}-D-Iva^{16}-L-Gln^{17}-L-Leuol^{18}, and the compound was given the trivial name trichorzin NPDG E (**5**). A right-handed helical conformation was assigned to **5** based

https://dx.doi.org/10.1021/acs.jnatprod.0c01370
J. Nat. Prod. 2021, 84, 503−517

on the appearance of negative Cotton effects at 208 and 225 nm observed in its ECD spectrum (Figure 2A).

Compound **6** was obtained as a colorless solid. The HRESIMS data were consistent with the molecular formula $C_{68}H_{117}N_{15}O_{17}$. The ^{1}H and ^{13}C NMR data for **6** supported the results of the mass spectrometry experiment indicating that the compound was a peptaibol; however, it was smaller than metabolites **1**−**5**. The ^{13}C NMR of **6** revealed 15 carbonyl resonances (δ_C 171−178 ppm), while the HSQC, HMBC, and COSY spectra suggested the compound likely contained 14 amino acid residues including Asn, Ser, Aib, Pro, Val, Iva, Leu, and Leuol (Figure S6). The sequence of amino acid residues in **6** was established using HMBC and ROESY correlation data and confirmed to be Ac-Iva^{1}-Asn^{2}-Leu^{3}-Aib^{4}-Pro^{5}-Ser^{6}-Val^{7}-Aib^{8}-Pro^{9}-Aib^{10}-Leu^{11}-Aib^{12}-Pro^{13}-Leuol^{14}. The tentative structure of **6** was further supported by MS/MS data, which contained several intense fragment ion peaks at *m*/*z* 454 (Ac-Aib^{4}) and 963 (Pro^{5}-Leuol^{14}), *m*/*z* 822 (Ac-Aib^{8}) and 595 (Pro^{9}-Leuol^{14}), and *m*/*z* 1202 (Ac-Aib^{12}) and 215 (Pro^{13}-Leuol^{14}). We conjectured that these abundant ions stemmed from the cleavage of one or both MS-labile bonds associated with the Aib and Pro residues. Notably, the same MS data pattern was observed for compound **20**, which had been obtained from the same fungal isolate and dereplicated as the metabolite harzianin HC I.[32] Comparison of the MS and NMR data for the two compounds indicated that the Aib^{2} residue in **20** had been changed to Iva^{2} in **6**. Marfey's method was used to secure the absolute configurations of the amino acids bearing stereogenic centers in **6**, which led to the conclusion that the structure of the metabolite was Ac-D-Iva^{1}-L-Asn^{2}-L-Leu^{3}-Aib^{4}-L-Pro^{5}-L-Ser^{6}-L-Val^{7}-Aib^{8}-L-Pro^{9}-Aib^{10}-L-Leu^{11}-Aib^{12}-L-Pro^{13}-L-Leuol^{14}. Metabolites **6** was given the trivial name harzianin NPDG A. An examination of the ECD data for **6** supported its conformation as a right-handed helix based on the appearance of negative Cotton effects at 205 and 230 nm (Figure 2B).[28−30]

Compound **7** was isolated as a colorless solid, and its molecular formula was determined to be $C_{69}H_{119}N_{15}O_{17}$ based on interpretation of its HRESIMS data. Analysis of the MS/MS and 1D and 2D NMR for **7** led to the realization that this peptaibol was structurally similar to harzianin HC XI (**22**).[32] A key structural difference between the two compounds was supported by the presence of a fragment ion at *m*/*z* 256 (Ac-Aib^{1}-Gln^{2}) in **7** and ^{13}C NMR chemical shift data that led to the conclusion that the Asn residue in **22** was replaced by a Gln. Using Marfey's and GITC methods, the absolute configuration of **7** was determined to be Ac-Aib^{1}-L-Gln^{2}-L-Leu^{3}-Aib^{4}-L-Pro^{5}-L-Ser^{6}-L-Ile^{7}-Aib^{8}-L-Pro^{9}-Aib^{10}-L-Leu^{11}-Aib^{12}-L-Pro^{13}-L-Leuol^{14}, and it was given the name harzianin NPDG B. The ECD data for **7** supported its conformation as a right-handed helix (Figure 2B).

Compound **8** was obtained as a colorless solid, and its molecular formula ($C_{69}H_{119}N_{15}O_{17}$) was established from HRESIMS data. Examination of the ^{13}C NMR and HSQC data for **8** revealed the metabolite shared many structural features with **6**; however, key differences were observed including the resonances attributable to Val^{7} in **6** were replaced in **8** by peaks corresponding to an Ile residue. Further investigation of the HMBC and ROESY correlation data for compound **8**, as well as results from its MS/MS fragmentation pattern, supported the proposed amino acid residue sequence Ac-Iva^{1}-Asn^{2}-Leu^{3}-Aib^{4}-Pro^{5}-Ser^{6}-Ile^{7}-Aib^{8}-Pro^{9}-Aib^{10}-Leu^{11}-Aib^{12}-Pro^{13}-Leuol^{14}. Further investigation of **8** using Marfey's and GITC methods established its absolute configuration as Ac-D-Iva^{1}-L-Asn^{2}-L-Leu^{3}-Aib^{4}-L-Pro^{5}-L-Ser^{6}-L-Ile^{7}-Aib^{8}-L-Pro^{9}-Aib^{10}-L-Leu^{11}-Aib^{12}-L-Pro^{13}-L-Leuol^{14}, and it was assigned the trivial name harzianin NPDG C. The ECD data for **8** were examined (Figure 2B), and the results were consistent with a right-handed helical conformation.

Compound **9** was obtained as a colorless solid, and its HRESIMS data were consistent with the molecular formula $C_{70}H_{121}N_{15}O_{17}$. Based on the substantial similarities among the MS, ^{1}H NMR, HSQC, and HMBC data for **9** and co-occurring metabolites **8** and harzianin HC XII (**23**),[32] it was concluded that one of the Aib residues had been replaced by an Iva in **9** (i.e., δ_H 8.44, 8.28, and 8.19 for N*H* of Aib residues and δ_H 9.80 and 7.89 attributed to N*H* of Iva residues). Examination of the MS/MS data identified a fragment ion at *m*/*z* 1032 (Ac-Iva^{10}), securing the position of the new Iva residue. HMBC and ROESY data, along with Marfey's and GITC analyses (Figure S9), were used to resolve the structure of **9** as Ac-D-Iva^{1}-L-Asn^{2}-L-Leu^{3}-Aib^{4}-L-Pro^{5}-L-Ser^{6}-L-Ile^{7}-Aib^{8}-L-Pro^{9}-D-Iva^{10}-L-Leu^{11}-Aib^{12}-L-Pro^{13}-L-Leuol^{14}, and the compound was given the trivial name harzianin NPDG D. Evidence concerning the solution conformation of **9** were obtained through the analysis of ECD data and were found to be consistent with expectations for a right-handed helix (Figure 2B).

Compound **10** was obtained as a colorless solid, and its HRESIMS data were used to assign it the molecular formula $C_{69}H_{119}N_{15}O_{16}$. Based on the observation that compound **10** contained one less oxygen atom than co-occurring metabolite **7**, the HSQC data for both compounds were comparatively probed, revealing that a signal attributable to a hydroxymethyl group in **7** (δ_C 62.1) had been replaced by a new methyl group (δ_C 16.8) in **10**. Considering how this change would manifest itself in the structure of **10**, it was determined that the most probable solution involved substituting the Ser residue in **7** with an Ala residue in metabolite **10**. Subsequent analysis of data from HMBC, ROESY, and MS/MS experiments confirmed this change, as well as helped to establish the amino acid sequence of **10**. Marfey's and GITC methods were used to establish the absolute configurations of its amino acid residues (Figure S10). Accordingly, the structure of peptaibol **10** was determined to be Ac-Aib^{1}-L-Gln^{2}-L-Leu^{3}-Aib^{4}-L-Pro^{5}-L-Ala^{6}-L-Ile^{7}-Aib^{8}-L-Pro^{9}-Aib^{10}-L-Leu^{11}-Aib^{12}-L-Pro^{13}-L-Leuol^{14}, and it was given the trivial name harzianin NPDG E. Compound **10** was determined to have a right-handed helical conformation as determined via analysis of its ECD data (Figure 2B).

Compound **11** was purified as a colorless solid, and it was assigned the molecular formula $C_{70}H_{121}N_{15}O_{16}$ based on interpretation of its HRESIMS data. An examination of the 1D and 2D NMR of **11** revealed that it was structurally similar to compound **10**; however, one of the Aib residues had been replaced by an Iva residue. Further scrutiny of the HMBC data indicated that the new Iva residue was positioned at the acetylated N-terminus of **11**. A combination of ROESY and MS/MS data was used to secure the sequence of **11**, while Marfey's and GITC methods were used to establish its absolute configuration as Ac-D-Iva^{1}-L-Gln^{2}-L-Leu^{3}-Aib^{4}-L-Pro^{5}-L-Ala^{6}-L-Ile^{7}-Aib^{8}-L-Pro^{9}-Aib^{10}-L-Leu^{11}-Aib^{12}-L-Pro^{13}-L-Leuol^{14}. Compound **11** was assigned the trivial name harzianin NPDG F. Metabolite **11** was proposed to possess a right-handed helical conformation based on data acquired from an ECD experiment (Figure 2B).

https://dx.doi.org/10.1021/acs.jnatprod.0c01370
J. Nat. Prod. 2021, 84, 503−517

Compound **12** was purified as a colorless solid. HRESIMS analysis revealed a doubly charged quasimolecular ion that was consistent with the molecular formula $C_{70}H_{121}N_{15}O_{16}$. Analysis of 1D and 2D NMR spectroscopic data for **12** revealed its high degree of similarity to **9** with the exception that the Ser[6] residue had been replaced by an Ala residue. Marfey's and GITC methods were used to establish the identities and absolute configurations of the amino acid residues in peptaibol **12** as Ac-D-Iva[1]-L-Asn[2]-L-Leu[3]-Aib[4]-L-Pro[5]-L-Ala[6]-L-Ile[7]-Aib[8]-L-Pro[9]-D-Iva[10]-L-Leu[11]-Aib[12]-L-Pro[13]-L-Leuol[14], and it was given the trivial name harzianin NPDG G. Analysis of the ECD spectrum of **12** revealed Cotton effects (Figure 2B) that were consistent with the metabolite possessing a right-handed helical conformation.

Compound **13** was obtained as a colorless solid, and its HRESIMS data were consistent with the molecular formula $C_{71}H_{123}N_{15}O_{16}$. Based on the analysis of its 1D and 2D NMR spectroscopy data, the structure of **13** was proposed to be similar to **12**. The major difference was that the Asn[2] residue in **12** was replaced by a Gln residue in **13**. Further investigation of the MS/MS, HMBC, and ROESY data helped secure the amino acid sequence of **13**, while the absolute configurations of its chiral amino acid residues were established using Marfey's and GITC methods. Thus, the structure of **13** was determined to be Ac-D-Iva[1]-L-Gln[2]-L-Leu[3]-Aib[4]-L-Pro[5]-L-Ala[6]-L-Ile[7]-Aib[8]-L-Pro[9]-D-Iva[10]-L-Leu[11]-Aib[12]-L-Pro[13]-L-Leuol[14], and it was given the trivial name harzianin NPDG H (**13**). The ECD spectrum of **13** exhibited Cotton effects similar to the other co-occurring metabolites (Figure 2B), which were consistent with a peptaibol bearing a right-handed helical conformation.

Compound **14** was obtained as a colorless solid, and it was assigned the molecular formula $C_{59}H_{104}N_{12}O_{13}$ based on interpretation of its HRESIMS data. The ^{13}C NMR and HMBC data for **14** confirmed the presence of 59 unique carbon atoms including 11 amide carbonyl resonances (δ_C ~170.0−180.0). Those data indicated that metabolite **14** contained fewer amino acid residues compared to peptaibols **1**−**13**. Further analysis of the 1D and 2D NMR data set revealed that **14** was structurally similar to harzianin HB I (**27**),[33] but the Aib[1]-Asn[2] residues in **27** had been replaced by Iva[1]-Gln[2] in **14**. The HMBC and ROESY correlation data were further probed, thus establishing the sequence of **14**, while Marfey's and GITC methods were used to confirm the absolute configurations of its chiral amino acids resulting in the proposed structure Ac-D-Iva[1]-L-Gln[2]-L-Leu[3]-L-Ile[4]-Aib[5]-L-Pro[6]-D-Iva[7]-L-Leu[8]-Aib[9]-L-Pro[10]-L-Leuol[11]. Metabolite **14** was given the trivial name harzianin NPDG I, and it was determined to possess a right-handed helical conformation based on interpretation of the results of ECD data (Figure 2C).[28−30]

Based on our investigation, natural products **1**−**14** had not been previously reported; however, these metabolites possessed structural features enabling their assignments to previously described families/subfamilies of peptaibols. For the sake of simplicity and clarity, we have used the predominant familial name of each peptaibol and added the cognominal term "NPDG" (Natural Products Discovery Group) to retain information pertaining to the structural relationship of each compound to the known co-occurring metabolites reported from this fungal genus, which included five trichorzin-HA-type peptaibols [trichorzin HA I (**15**),[24,25] trichorzin HA II (**16**),[24,25] trichorzin HA V (**17**),[24,25] trichorzin HA VI (**18**),[24,25] and trichorzin HA VII (**19**),[24,25]], seven harzianin-HC-type peptaibols [harzianin HC I (**20**),[32] harzianin HC III (**21**),[32] harzianin HC XI (**22**),[32] harzianin HC XII (**23**),[32] harzianin HC XIV (**24**),[32] harzianin HC X (**25**),[32] and harzianin HC XV (**26**)[32]], and one harzianin-HB-type peptaibol [harzianin HB I (**27**)[33]]. This terminology is intended to help avoid further confusion associated with the circuitous naming history of these structurally diverse metabolites. The co-production of so many different peptaibol types from a single fungus is not entirely unusual; however, the combination of peptaibol diversity and abundance observed from this *Trichoderma* isolate offers a striking example of nature's capacity for biosynthetic promiscuity and structural experimentation.

Structure Elucidation of Peptaibols and Lipopeptaibols Isolated from *H. pachybasioides*. Compound **28** was obtained as a colorless solid, and its molecular formula was determined to be $C_{37}H_{69}N_7O_8$ based on interpretation of its HRESIMS data. An examination of the ^1H NMR data yielded evidence supporting the occurrence of several putative N$\underline{H}$ (δ_H 8.0−10.0 ppm) and α-protons (δ_H 3.7−5.0 ppm) that were indicative of seven amino acids in **28** (Figure S15). Analysis of the ^{13}C, HMBC, and COSY NMR data supported the presence of two Aib, two Gly, one Val, one Ile, and one Leuol residue, which left eight carbon atoms unaccounted for in **28**. Examination of the COSY and HMBC correlation data attributable to the remaining carbon atoms led to the conclusion that they formed an *n*-octanoyl moiety. A combination of HMBC and ROESY correlation data along with MS/MS fragmentation results were employed to construct the sequence of **28**: *n*-Oct-Aib[1]-Gly[2]-Val[3]-Aib[4]-Gly[5]-Ile[6]-Leuol[7]. The absolute configurations of the chiral amino acid residue were determined by Marfey's and GITC methods, which established the structure of metabolite **28** as *n*-Oct-Aib[1]-Gly[2]-L-Val[3]-Aib[4]-Gly[5]-L-Ile[6]-L-Leuol[7]. Notably metabolite **28**, which was given the trivial name hypocrin NPDG A, is a notable addition to an uncommon subfamily of *n*-Oct-peptaibols (lipopeptaibols); it contains a smaller number of amino acid residues (seven amino acids) as compared to the more commonly encountered members of the group, which contain 11 amino acids.[34−37] Interpretation of the ECD data for **28** indicated that this compound did not exhibit a right-handed helical conformation (Figure 2D) like the other metabolites from the *Trichoderma* isolate. We speculated that the reduced length of the amino acid residue chain was too short for this compound to adopt distinctive secondary structural features, and instead, it remained a random coil.[38−40]

Compound **29** was isolated as a colorless solid, and its molecular formula was established as $C_{37}H_{69}N_7O_8$ based on interpretation of its HRESIMS data. The molecular formula of **29** was identical to that for metabolite **28**, which provided an initial indication that these compounds might be structurally related. An inspection of the 1D and 2D NMR data revealed that the Val[3] and Ile[6] residues in **28** had been replaced by Leu[3] and Val[6] residues in **29**. Using Marfey's method, the absolute configurations of the chiral amino acids were established, resulting in the structure elucidated as *n*-Oct-Aib[1]-Gly[2]-L-Leu[3]-Aib[4]-Gly[5]-L-Val[6]-L-Leuol[7]. Lipopeptaibol **29** was given the trivial name hypocrin NPDG B. Analysis of the ECD data indicated that compound **29** did not possess a defined secondary structure and was instead a random coil (Figure 2D).

Compound **30** was obtained as a colorless solid, and its HRESIMS data were consistent with the molecular formula $C_{38}H_{71}N_7O_8$. In comparison to metabolite **29**, compound **30**

https://dx.doi.org/10.1021/acs.jnatprod.0c01370
J. Nat. Prod. 2021, 84, 503−517

contained the equivalent of one additional $-CH_2-$ unit. Upon examining the HMBC and ROESY data, it was determined that these atoms were incorporated into what had formerly been the Val residue in compound **29**, resulting in a new Ile residue in **30**. Further examination of the structure of the molecule using 1D and 2D NMR experiments, MS/MS fragmentation data, and Marfey's and GITC methods yielded evidence supporting the structure of **30** as *n*-Oct-Aib[1]-Gly[2]-L-Leu[3]-Aib[4]-Gly[5]-L-Ile[6]-L-Leuol[7]. Lipopeptaibol **30** was given the trivial name hypocrin NPDG C. The ECD spectrum of **30** offered no evidence supporting the presence of a defined secondary structure for this metabolite (Figure 2D).

Compound **31** was purified as a colorless solid, and it was assigned the molecular formula $C_{49}H_{89}N_{11}O_{12}$ based on interpretation of its HRESIMS data. Examination of the 1D and 2D NMR data for **31** confirmed the presence of four additional amino acid residues in this metabolite compared to co-occurring metabolites **28**−**30**. A combination of HMBC and ROESY correlation data, MS/MS fragmentation analysis, and Marfey's method was used to establish the structure of **31** as *n*-Oct-Aib[1]-Gly[2]-L-Val[3]-Aib[4]-Gly[5]-Gly[6]-L-Val[7]-Aib[8]-Gly[9]-L-Val[10]-L-Leuol[11], and the metabolite was given the trivial name hypocrin NPDG D. Compound **31** was subjected to ECD spectroscopy, which revealed negative Cotton effects at 206 and 223 nm that were indicative of a right-handed helical conformation (Figure 2E).

Compound **32** was obtained as a colorless solid, and interpretation of its HRESIMS data supported the molecular formula $C_{50}H_{91}N_{11}O_{12}$. Inspection of the 1D NMR data for **32** revealed many of the chemical shifts in this compound were similar to those found in lipopeptaibol **31**. An investigation of **32** using HMBC and ROESY correlation data, MS/MS fragmentation analysis, and Marfey's method led to its assignment as *n*-Oct-Aib[1]-Gly[2]-L-Leu[3]-Aib[4]-Gly[5]-Gly[6]-L-Val[7]-Aib[8]-Gly[9]-L-Val[10]-L-Leuol[11], and it was given the trivial name hypocrin NPDG E. The ECD spectrum of **32** was dominated by two negative Cotton effects characteristic for compounds that adopt right-handed helical conformations (Figure 2E).

Compounds **33**−**35** were obtained as colorless solids, and all three compounds were determined to share the molecular formula $C_{51}H_{93}N_{11}O_{12}$ based on interpretation of their HRESIMS data. A preliminary examination of the 1D and 2D data for each of the three compounds revealed that they were structurally similar to one another and were analogues of co-occurring lipopeptaibols **31** and **32**. Using this information to guide the structure determination process, the structures of **33**−**35** were solved in parallel using a combination of 1D and 2D NMR data, MS/MS fragmentation analysis, and Marfey's and GITC methods. The resulting structures of the compounds were determined to be *n*-Oct-Aib[1]-Gly[2]-L-Leu[3]-Aib[4]-Gly[5]-Gly[6]-L-Val[7]-Aib[8]-Gly[9]-L-Leu[10]-L-Leuol[11] (**33**), *n*-Oct-Aib[1]-Gly[2]-L-Leu[3]-Aib[4]-Gly[5]-Gly[6]-L-Val[7]-Aib[8]-Gly[9]-L-Ile[10]-L-Leuol[11] (**34**), and *n*-Oct-Aib[1]-Gly[2]-L-Val[3]-Aib[4]-Gly[5]-Gly[6]-L-Leu[7]-Aib[8]-Gly[9]-L-Ile[10]-L-Leuol[11] (**35**), which were assigned the trivial names hypocrins NPDG F, G, and H, respectively. Compounds **33**−**35** were probed using ECD spectroscopy, which revealed Cotton effect patterns similar to lipopeptaibols **31** and **32**. Accordingly, a right-handed helical conformation was assigned to **33**−**35** (Figure 2E).

Compound **36** was obtained as a colorless solid. The HRESIMS data for **36** were interpreted to support the molecular formula $C_{52}H_{95}N_{11}O_{12}$. Examination of the 1D and 2D NMR revealed that unlike compounds **31**−**35**, metabolite **36** appeared to contain no Val or Ile residues at positions 3, 7, or 10. Instead, these amino acid residues had been replaced by Leu residues. Upon determining the sequence of **36**, Marfey's method was used to determine the absolute configurations of the chiral amino acids. Based on interpretation of data from those experiments, the structure of **36** was established as *n*-Oct-Aib[1]-Gly[2]-L-Leu[3]-Aib[4]-Gly[5]-Gly[6]-L-Leu[7]-Aib[8]-Gly[9]-L-Leu[10]-L-Leuol[11], and it was given the trivial name hypocrin NPDG I. Analysis of the ECD spectrum for **36** revealed negative Cotton effects at 206 and 223 nm, indicative of a right-handed helical conformation (Figure 2E).

Compound **37** appeared as a colorless solid, and its molecular formula ($C_{63}H_{113}N_{15}O_{16}$) was assigned based on analysis of its HRESIMS data. Compared to metabolites **30**−**36**, compound **37** was larger, with the ^{13}C NMR and HMBC data supporting the presence of 15 putative amide carbonyls (δ_C ~170−180 ppm). Using 1D and 2D NMR data, as well as MS/MS fragmentation data, the sequence of **37** was established, while Marfey's and GITC methods were used to verify the absolute configurations of the chiral amino acid residues. Based on interpretation of the data from these experiments, the structure of lipopeptaibol **37** was determined to be *n*-Oct-Aib[1]-Gly[2]-L-Val[3]-Aib[4]-Gly[5]-Gly[6]-L-Val[7]-Aib[8]-Gly[9]-Gly[10]-L-Val[11]-Aib[12]-Gly[13]-L-Ile[14]-L-Leuol[15], and it was given the trivial name hypocrin NPDG J. The ECD data for **37** were consistent with those expected for a peptide possessing a right-handed helical conformation based on the appearance of negative Cotton effects at 206 and 222 nm (Figure 2F).

Compounds **38**, **39**, and **40** were purified as colorless solids that shared the same molecular formula ($C_{64}H_{115}N_{15}O_{16}$) based on interpretation of their HRESIMS data. Analysis of the 1D and 2D NMR data indicated that compounds **38**, **39**, and **40** possessed similar amino acid patterns consisting of *n*-Oct-Aib[1]-Gly[2]-(Val or Leu)[3]-Aib[4]-Gly[5]-Gly[6]-(Val or Leu)[7]-Aib[8]-Gly[9]-Gly[10]-(Val or Leu)[11]-Aib[12]-Gly[13]-Ile[14]-L-Leuol[15]. Focusing on 2D NMR correlation data for the variable portions of each compound (amino acid residue positions 3, 7, and 11), it was determined that lipopeptaibol **38** was composed of Leu[3], Val[7], and Val[11], lipopeptaibol **39** comprised Val[3], Leu[7], and Val[11], and lipopeptaibol **40** comprised Val[3], Val[7], and Leu[11]. With the sequences of **38**−**40** established, Marfey's and GITC methods were used to secure the absolute configurations of the chiral amino acid, resulting in the following structure assignments: *n*-Oct-Aib[1]-Gly[2]-L-Leu[3]-Aib[4]-Gly[5]-Gly[6]-L-Val[7]-Aib[8]-Gly[9]-Gly[10]-L-Val[11]-Aib[12]-Gly[13]-L-Ile[14]-L-Leuol[15] (**38**), *n*-Oct-Aib[1]-Gly[2]-L-Val[3]-Aib[4]-Gly[5]-Gly[6]-L-Leu[7]-Aib[8]-Gly[9]-Gly[10]-L-Val[11]-Aib[12]-Gly[13]-L-Ile[14]-L-Leuol[15] (**39**), and *n*-Oct-Aib[1]-Gly[2]-L-Val[3]-Aib[4]-Gly[5]-Gly[6]-L-Val[7]-Aib[8]-Gly[9]-Gly[10]-L-Leu[11]-Aib[12]-Gly[13]-L-Ile[14]-L-Leuol[15] (**40**). These compounds were assigned the trivial names hypocrins NPDG K (**38**), L (**39**), and M (**40**). The ECD spectra for peptaibols **38**−**40** exhibited negative Cotton effects at 206 and 222 nm (Figure 2F), indicative of right-handed helical conformations. Additionally, colorless block-shaped crystals of compound **40** were obtained and subjected to single-crystal X-ray diffraction analysis, which served to independently confirm the structure and conformation of this lipopeptaibol (Figure 3).

Compounds **41**, **42**, and **43** were obtained as colorless solids, which shared the molecular formula $C_{65}H_{117}N_{15}O_{16}$ based on analyses of their HRESIMS data. Comparisons of the 1D and 2D NMR data and MS/MS fragmentation results for **41**−**43** versus **38**−**40** led to the determination that the structures of these metabolites were similar; however, each

https://dx.doi.org/10.1021/acs.jnatprod.0c01370
J. Nat. Prod. 2021, 84, 503−517

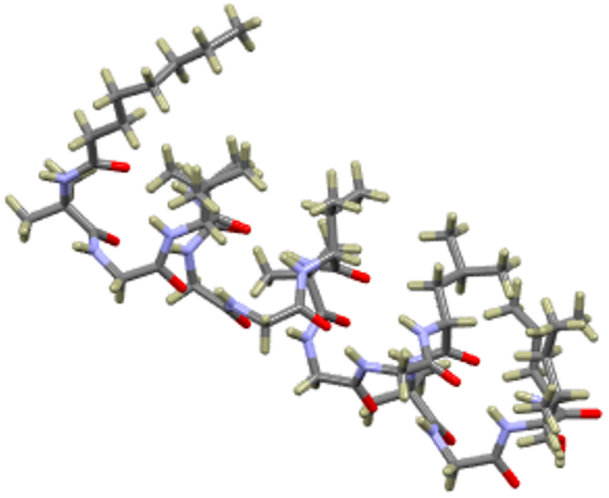

Figure 3. Helical structure of **40** as determined by single-crystal X-ray diffraction analysis.

member of the new compound set (**41**−**43**) possessed new Leu residues in place of the Val residues in **38**−**40**. The structures of the lipopeptaibols were established based on interpretation of 1D and 2D NMR data in combination with results from Marfey's and GITC experiments to give *n*-Oct-Aib[1]-Gly[2]-L-Val[3]-Aib[4]-Gly[5]-Gly[6]-L-Leu[7]-Aib[8]-Gly[9]-Gly[10]-L-Leu[11]-Aib[12]-Gly[13]-L-Ile[14]-L-Leuol[15] (**41**), *n*-Oct-Aib[1]-Gly[2]-L-Leu[3]-Aib[4]-Gly[5]-Gly[6]-L-Val[7]-Aib[8]-Gly[9]-Gly[10]-L-Leu[11]-Aib[12]-Gly[13]-L-Ile[14]-L-Leuol[15] (**42**), and *n*-Oct-Aib[1]-Gly[2]-L-Leu[3]-Aib[4]-Gly[5]-Gly[6]-L-Leu[7]-Aib[8]-Gly[9]-Gly[10]-L-Val[11]-Aib[12]-Gly[13]-L-Ile[14]-L-Leuol[15] (**43**). The compounds were given the trivial names hypocrins NPDG N (**41**), O (**42**), and P (**43**). Lipopeptaibols **41**−**43** were subjected to ECD experiments, and the compounds were determined to possess right-handed helical conformations based on the negative Cotton effects at 206 and 222 nm (Figure 2F).

To the best of our knowledge, natural products **28**−**43** had not been previously reported, but these lipopeptaibols are structurally similar to other well-established families and subfamilies of peptidic fungal natural products. As previously described (*vide supra*), we attempted to match the new metabolites described in this report with existing compound names, while avoiding the perpetuation of awkward alphanumeric codes, by adding the term "NPDG" to each new name. In addition to metabolites **28**−**43**, several additional peptaibols and lipopeptaibols were purified from the *H. pachybasioides* extract and dereplicated by comparisons to reported spectroscopic data. The compounds dereplicated in this manner included trikoningin KB I (**44**),[41] trichogin A IV (**45**),[42] trichogin GB IX (**46**),[43] trichosporin B IIId (**47**),[44] trichosporin B IIIa (**48**),[44] trichosporin B IVc (**49**),[45] trichosporin B VIb (**50**),[46] trichosporin B VIa (**51**),[46] and trichosporin B VIIa (**52**).[46]

Testing the Antiplasmodial Activities of Fungal-Derived Peptidic Natural Products. The 52 peptaibols and lipopetaibols purified from *T. harzianum* and *H. pachybasioides*, along with two additional fungal peptides from the University of Oklahoma Natural Products Discovery Group pure compound library [efrapeptins F (**53**) and G (**54**) were previously procured from a *Tolypocladium* sp. isolate[47]], were tested for their antiplasmodial activities. Tests were conducted using the multi-drug-resistant *P. falciparum* line Dd2, while a cytotoxicity counter screen was performed using human (HepG2) hepatocytes. All of the compounds exhibited varying degrees of inhibition of *P. falciparum*, with several compounds (**10**, **11**, **13**, **14**, **48**, **51**, and **53**) demonstrating potent, submicromolar activities (Tables 1−8).

Further exploration of the data to determine how particular molecular features of the individual metabolites (e.g., presence or absence of specific amino acid residues and the order in

Table 2. Inhibitory Effects of 14-AA Peptaibols (6−13 and 20−26)

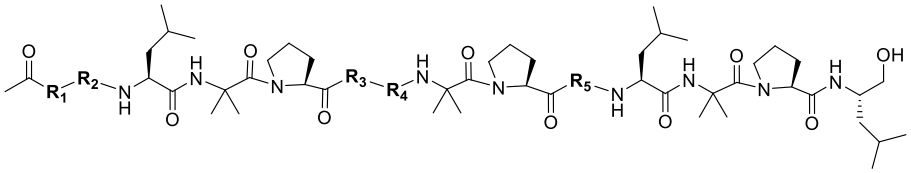

compound	MW	R_1	R_2	R_3	R_4	R_5	*P. falciparum* EC_{50} (μM)[a]	HepG2 EC_{50} (μM)[a]	SI
harzianin NPDG A (**6**)	1415	D-Iva	L-Asn	L-Ser	L-Val	Aib	0.62 ± 0.06	>25	>40
harzianin NPDG B (**7**)	1429	Aib	L-Gln	L-Ser	L-Ile	Aib	1.75 ± 0.12	>25	>14
harzianin NPDG C (**8**)	1429	D-Iva	L-Asn	L-Ser	L-Ile	Aib	0.58 ± 0.06	>25	>43
harzianin NPDG D (**9**)	1443	D-Iva	L-Asn	L-Ser	L-Ile	D-Iva	0.52 ± 0.04	>25	>48
harzianin NPDG E (**10**)	1413	Aib	L-Gln	L-Ala	L-Ile	Aib	0.29 ± 0.02	>25	>86
harzianin NPDG F (**11**)	1427	D-Iva	L-Gln	L-Ala	L-Ile	Aib	0.32 ± 0.01	>25	>78
harzianin NPDG G (**12**)	1427	D-Iva	L-Asn	L-Ala	L-Ile	D-Iva	0.62 ± 0.01	>25	>40
harzianin NPDG H (**13**)	1441	D-Iva	L-Gln	L-Ala	L-Ile	D-Iva	0.33 ± 0.09	>25	>76
harzianin HC I (**20**)	1401	Aib	L-Asn	L-Ser	L-Val	Aib	0.71 ± 0.08	>25	>35
harzianin HC III (**21**)	1415	Aib	L-Asn	L-Ser	L-Val	D-Iva	0.56 ± 0.07	>25	>45
harzianin HC XI (**22**)	1415	Aib	L-Asn	L-Ser	L-Ile	Aib	0.63 ± 0.08	>25	>40
harzianin HC XII (**23**)	1429	Aib	L-Asn	L-Ser	L-Ile	D-Iva	0.52 ± 0.05	>25	>48
harzianin HC XIV (**24**)	1399	Aib	L-Asn	L-Ala	L-Ile	Aib	0.42 ± 0.03	>25	>60
harzianin HC X (**25**)	1413	Aib	L-Gln	L-Ala	L-Val	D-Iva	1.32 ± 0.08	>25	>19
harzianin HC XV (**26**)	1427	Aib	L-Gln	L-Ala	L-Ile	D-Iva	0.63 ± 0.08	>25	>40

[a]Results are expressed as means from triplicate experiments.

https://dx.doi.org/10.1021/acs.jnatprod.0c01370
J. Nat. Prod. 2021, 84, 503−517

Table 3. Inhibitory Effects of 11-AA Peptaibols (14 and 27)

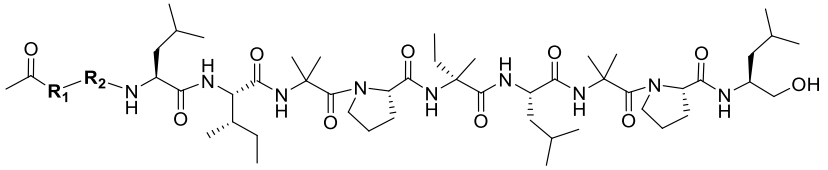

compound	MW	R_1	R_2	*P. falciparum* EC_{50} (μM)[a]	HepG2 EC_{50} (μM)[a]	SI
harzianin NPDG I (**14**)	1188	D-Iva	L-Gln	0.10 ± 0.01	>25	>250
harzianin HB I (**27**)	1160	Aib	L-Asn	0.72 ± 0.13	>25	>35

[a]Results are expressed as means from triplicate experiments.

Table 4. Inhibitory Effects of 7-AA Lipopeptaibols (28−30)

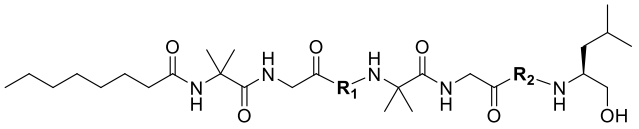

compound	MW	R_1	R_2	*P. falciparum* EC_{50} (μM)[a]	HepG2 EC_{50} (μM)[a]	SI
hypocrin NPDG A (**28**)	739	L-Val	L-Ile	1.12 ± 0.05	>25	>22
hypocrin NPDG B (**29**)	739	L-Leu	L-Val	3.00 ± 0.15	>25	>8
hypocrin NPDG C (**30**)	753	L-Leu	L-Ile	2.90 ± 0.22	>25	>9

[a]Results are expressed as means from triplicate experiments.

which the amino acids appeared) impacted biological activity proved unfruitful at detecting decisive structure−activity trends. However, some notable patterns emerged when the data were considered in aggregate based on their classification into eight groups: peptaibols composed of 11 amino acid residues (group A), peptaibols composed of 14 amino acid residues (group B), peptaibols composed of 18 amino acid residues (group C), peptaibols composed of 20 amino acid residues (group D), lipopeptaibols composed of seven amino acid residues (group E), lipopeptaibols composed of 11 amino acid residues (group F), lipopeptaibols composed of 15 amino acid residues (group G), and efrapeptins (group H). Data visualization using a scatter plot (Figure 4) revealed that, in general, the lipopeptaibols (groups E, F, and G) were less potent against *P. falciparum* compared to the other groups of metabolites. In contrast, the efrapeptins (group H) showed tremendous potency and selectivity; however, with only two representatives available from this group, it is not known if our results are generalizable to all efrapeptins or might be outliers. Taken together, the peptaibols (groups A, B, C, and D) exhibited consistent inhibitory activity against *P. falciparum*. However, a more notable property of many peptaibols, especially groups A and B, was the selectivity exhibited toward the parasite versus human cells. Several of these metabolites (e.g., compounds **10**, **11**, **13**, **14**, and **24**) exhibited selectivity index values (SI = EC_{50} for HepG2 cells/EC_{50} for *P. falciparum*) that were > 60. The only compound from another group to achieve such a remarkable threshold was **53** from group H (SI > 64). These results indicate that peptaibols and lipopeptaibols are capable of eliciting divergent toxicity profiles across dissimilar organisms such as humans (Chordata) and Apicomplexa. These results provide a reasonable basis for optimism that further investigation of peptailbol and lipopeptaibol chemistry may offer additional potent inhibitors of *Plasmodium* spp. that exhibit little or no toxicity toward humans.

EXPERIMENTAL SECTION

General Experimental Procedures. Optical rotation measurements were made using a Rudolph Research Autopol III automatic polarimeter. NMR spectra were obtained on Varian NMR spectrometers (400 and 500 MHz for ^{1}H and 100 and 125 MHz for ^{13}C). HRESIMS data were obtained on an Agilent 6538 high-mass-resolution QTOF mass spectrometer. ECD spectra were obtained on a JASCO J-715 circular dichroism spectrometer. Vacuum

Table 5. Inhibitory Effects of 11-AA Lipopeptaibols (31−36, 44, and 45)

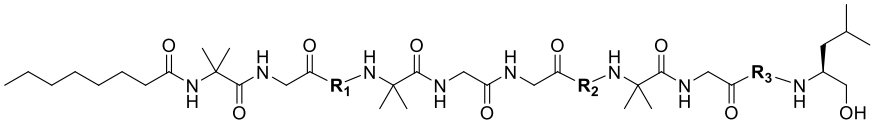

compound	MW	R_1	R_2	R_3	*P. falciparum* EC_{50} (μM)[a]	HepG2 EC_{50} (μM)[a]	SI
hypocrin NPDG D (**31**)	1023	L-Val	L-Val	L-Val	2.68 ± 0.10	>25	>9
hypocrin NPDG E (**32**)	1037	L-Leu	L-Val	L-Val	2.53 ± 0.31	>25	>10
hypocrin NPDG F (**33**)	1051	L-Leu	L-Val	L-Leu	0.89 ± 0.13	>25	>28
hypocrin NPDG G (**34**)	1051	L-Leu	L-Val	L-Ile	3.14 ± 0.13	>25	>8
hypocrin NPDG H (**35**)	1051	L-Val	L-Leu	L-Ile	1.93 ± 0.12	>25	>13
hypocrin NPDG I (**36**)	1065	L-Leu	L-Leu	L-Leu	2.38 ± 0.06	>25	>11
trikoningin KB I (**44**)	1037	L-Val	L-Val	L-Ile	0.91 ± 0.05	10.73 ± 1.47	12
trichogin A IV (**45**)	1065	L-Leu	L-Leu	L-Ile	0.93 ± 0.06	8.09 ± 1.07	9

[a]Results are expressed as means from triplicate experiments.

https://dx.doi.org/10.1021/acs.jnatprod.0c01370
J. Nat. Prod. 2021, 84, 503−517

Table 6. Inhibitory Effects of 15-AA Lipopeptaibols (37−43 and 46)

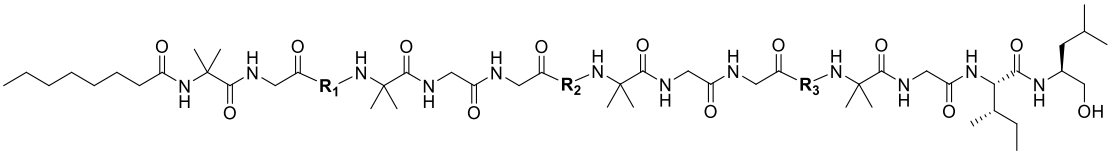

compound	MW	R_1	R_2	R_3	*P. falciparum* EC_{50} (μM)[a]	HepG2 EC_{50} (μM)[a]	SI
hypocrin NPDG J (**37**)	1335	L-Val	L-Val	L-Val	0.58 ± 0.06	>25	>43
hypocrin NPDG K (**38**)	1349	L-Leu	L-Val	L-Val	2.27 ± 0.20	>25	>11
hypocrin NPDG L (**39**)	1349	L-Val	L-Leu	L-Val	1.55 ± 0.22	>25	>16
hypocrin NPDG M (**40**)	1349	L-Val	L-Val	L-Leu	2.53 ± 0.10	>25	>10
hypocrin NPDG N (**41**)	1363	L-Val	L-Leu	L-Leu	2.10 ± 0.14	>25	>12
hypocrin NPDG O (**42**)	1363	L-Leu	L-Val	L-Leu	0.79 ± 0.09	23.55 ± 0.63	30
hypocrin NPDG P (**43**)	1363	L-Leu	L-Leu	L-Val	0.83 ± 0.13	>25	>30
trichogin A IV (**46**)	1377	L-Leu	L-Leu	L-Leu	0.58 ± 0.05	15.88 ± 0.64	27

[a]Results are expressed as means from triplicate experiments.

Table 7. Inhibitory Effects of 20-AA Peptaibols (47−52)

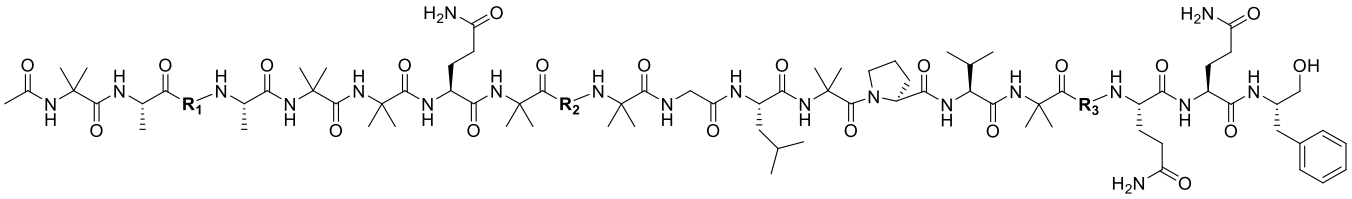

compound	MW	R_1	R_2	R_3	*P. falciparum* EC_{50} (μM)[a]	HepG2 EC_{50} (μM)[a]	SI
trichosporin B IIId (**47**)	1936	L-Ala	L-Val	Aib	0.56 ± 0.06	9.28 ± 0.84	17
trichosporin B IIIa (**48**)	1950	L-Ala	L-Leu	Aib	0.32 ± 0.02	5.77 ± 0.53	18
trichosporin B IVc (**49**)	1950	Aib	L-Val	Aib	0.58 ± 0.03	6.53 ± 0.74	11
trichosporin B VIb (**50**)	1964	L-Ala	L-Ile	D-Iva	0.52 ± 0.06	3.35 ± 0.25	6
trichosporin B VIa (**51**)	1964	Aib	L-Ile	Aib	0.37 ± 0.02	2.93 ± 0.21	8
trichosporin B VIIa (**52**)	1978	Aib	L-Ile	D-Iva	0.72 ± 0.02	3.78 ± 0.24	5

[a]Results are expressed as means from triplicate experiments.

Table 8. Inhibitory Effects of Peptides in the Pure Compound Library (53 and 54)

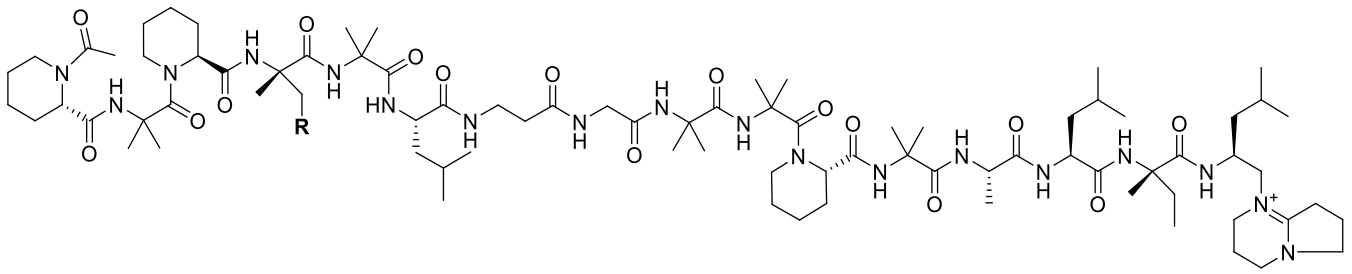

compound	M.W.	R	*P. falciparum* EC_{50} (μM)[a]	HepG2 EC_{50} (μM)[a]	SI	Source
efrapeptin F (**53**)	1635	H	0.39 ± 0.06	>25	>64	fungus: *Tolypocladium* sp.
efrapeptin G (**54**)	1649	CH_3	0.46 ± 0.05	>25	>54	fungus: *Tolypocladium* sp.

column chromatography was performed over silica gel (VWR, 40−60 μm, 6 Å) and HP20ss gel (Sorbtech). The preparative HPLC system was equipped with Shimadzu SCL-10A VP pumps and a system controller using a Gemini 5 μm C_{18} column (210 Å, 250 × 21.2 mm) with a flow rate of 10 mL/min. The semipreparative HPLC were conducted on a Waters system (1525 binary pumps and Waters 2998 photodiode array detectors) using a Gemini 5 μm C_{18} (110 Å, 250 × 10 mm), F5 (110 Å, 250 × 10 mm), or biphenyl column (110 Å, 250 × 10 mm) with a flow rate of 4 mL/min. All solvents used were of ACS grade or better.

Fungal Isolates and Fermentation. The *Trichoderma* sp. isolate (TX3005 RBM-20) was obtained from a soil sample collected near Galveston, Texas, USA, while the *Hypocrea* sp. isolate (PA4898 RBM-5) was obtained from a soil sample collected in the vicinity of Gilbertsville, Pennsylvania, USA. The fungi were identified by collecting mycelium and subjecting the samples to homogenization in TE buffer (10 mM Tris HCl, 0.1 mM EDTA, pH 8.0) with zirconium oxide beads in a Bullet blender (MidSci #BBY24M). The DNA was collected, and the ITS region (i.e., ITS1, 5.8S, and ITS2 regions) amplified by PCR for sequencing. The resulting sequence data were compared to fungal sequences contained in GenBank, which led to 100% identity matches to isolates described as *Trichoderma harzianum* (isolate from Galveston, Texas) and *Hypocrea pachybasioides* (isolate from Gilbertsville, Pennsylvania). Sequence

https://dx.doi.org/10.1021/acs.jnatprod.0c01370
J. Nat. Prod. 2021, 84, 503−517

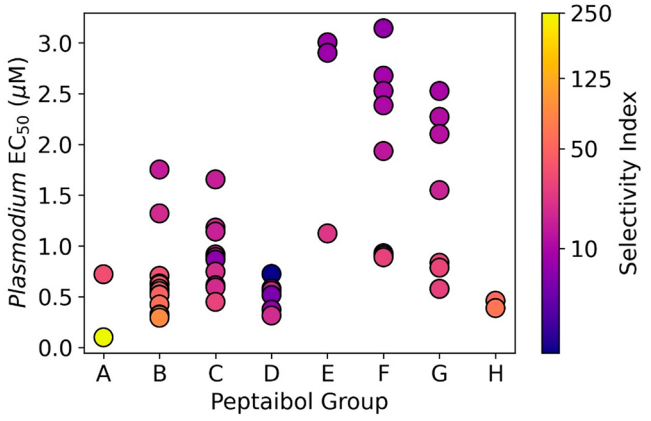

Figure 4. Scatter plot displaying antiplasmodial activity and selectivity afforded by 54 peptidic fungal natural products including peptaibols composed of 11 amino acid residues (**14** and **27**; group A), peptaibols composed of 14 amino acid residues (**6**−**13** and **20**−**26**; group B), peptaibols composed of 18 amino acid residues (**1**−**5** and **15**−**19**;group C), peptaibols composed of 20 amino acid residues (**47**−**52**; group D), lipopeptaibols composed of seven amino acid residues (**28**−**30**; group E), lipopeptaibols composed of 11 amino acid residues (**31**−**36** and **44**−**45**; group F), lipopeptaibols composed of 15 amino acid residues (**37**−**43** and **46**; group G), and efrapeptins (**53** and **54**; group H).

data were deposited in GenBank (*T. harzianum*: GenBank accession no. MK558706, and *H. pachybasioides*: GenBank accession no. MK883713). Based on our standard natural product dereplication procedures, extracts prepared from the two fungal isolates provided evidence [i.e., λ_{max} = 190−210, *m*/*z* values in the range of 700−2000, and t_R = 9−12 min (LC-MS method: C_{18}, gradient system from 10% to 100% MeCN in H_2O with 0.1% formic acid over 13 min, flow rate: 0.4 mL/min)] that peptidic natural products were the dominant type of metabolite in the samples under investigation.

To prepare the isolates for chemical studies, fungi were recovered from cryogenic storage (stored in a vial at −80 °C as mycelium with 20% aqueous glycerol). Following recovery on Czapek agar plates (30 g sucrose, 2 g $NaNO_3$, 1 g K_2HPO_4, 0.5 g $MgSO_4{\cdot}7H_2O$, 0.5 g KCl, 0.01 g $FeSO_4{\cdot}7H_2O$, 0.05 g chloramphenicol, 1 L DI H_2O), lawns of fungal mycelium were aseptically cut into small pieces (∼1 cm^2) for use as the scale-up culture inoculum. Scale-up cultures were carried out by charging mycobags (Unicorn Bags, Plano, TX, USA) with monolayers of Cheerios breakfast cereal supplemented with a 0.3% sucrose solution and 0.005% chloramphenicol. The pieces of mycelium were aseptically added to three mycobags per fungal isolate, and the cultures were grown at room temperature for 4 weeks.

Extraction and Isolation of *T. harzianum*. Fungal biomass was extracted with 2 L of EtOAc (×3) at room temperature, the organic solvent layers were recovered, and the solvent was removed under vacuum. The EtOAc-soluble material was combined for further processing (34 g, fraction A). Fraction A was subjected to silica gel vacuum column chromatography with elution performed using dichloromethane (fraction B), dichloromethane−MeOH (10:1) (fraction C), and MeOH (fraction D). Fraction D (10 g) was also further fractionated by HP20ss gel vacuum column chromatography into five samples: fractions E (30% MeOH), F (50% MeOH), G (70% MeOH), H (90% MeOH), and I (100% MeOH). Fraction H (5 g) was further subjected to preparative HPLC (C_{18}, gradient elution with 85−100% MeOH in H_2O over 15 min using a 10 mL/min flow rate) to afford seven subfractions (H1−H7). Subfraction H1 (300 mg) was subjected to preparative HPLC (C_{18}, gradient elution with 85−100% MeCN−H_2O over 15 min using a 10 mL/min flow rate) to afford 12 subfractions (H1-1−H1-12). Compound **20** (2 mg, t_R = 10 min) was purified from subfraction H1-2 (10 mg) by semipreparative HPLC [F5, isocratic MeCN−H_2O (42.5:57.5), flow rate: 4 mL/min]. Subfraction H1-3 (20 mg) was obtained by semipreparative HPLC [F5, isocratic MeCN−H_2O (42.5:57.5), flow rate: 4 mL/min] to give compounds **21** (2.5 mg, t_R = 11 min) and **6** (2.3 mg, t_R = 12 min). Compound **22** (5 mg, t_R = 12 min) was purified from subfraction H1-4 (20 mg) by semipreparative HPLC [F5, isocratic MeCN−H_2O (42.5:57.5), flow rate: 4 mL/min]. Subfraction H1-5 (35 mg) was subjected to semipreparative HPLC [F5, isocratic MeCN−H_2O (42.5:57.5), flow rate: 4 mL/min], yielding compounds **7** (3 mg, t_R = 14 min), **23** (6 mg, t_R = 15 min), and **8** (6 mg, t_R = 16 min). Compound **9** (10 mg, t_R = 7 min) was purified from subfraction H1-6 (35 mg) by semipreparative HPLC [C_{18}, isocratic MeCN−H_2O (42.5:57.5), flow rate: 4 mL/min]. Subfraction H1-8 (30 mg) was further subjected to semipreparative HPLC [F5, isocratic MeCN−H_2O (45:55), flow rate: 4 mL/min] to yield compounds **24** (2 mg, t_R = 8 min), **25** (2 mg, t_R = 10 min), and **27** (3 mg, t_R = 12 min). Subfraction H1-9 (30 mg) was purified by semipreparative HPLC [F5, isocratic MeCN−H_2O (47.5:52.5), flow rate: 4 mL/min] to give compounds **10** (2 mg, t_R = 8 min) and **11** (2 mg, t_R = 11 min). Subfraction H1-10 (20 mg) was further purified by semipreparative HPLC [F5, isocratic MeCN−H_2O (47.5:52.5), flow rate: 4 mL/min] to yield compounds **26** (5 mg, t_R = 10 min), **12** (5 mg, t_R = 11 min), and **14** (1.5 mg, t_R = 13 min). Compound **13** (3 mg, t_R = 12 min) was purified from subfraction H1-11 (25 mg) by semipreparative HPLC [F5, isocratic MeCN−H_2O (47.5:52.5), flow rate: 4 mL/min]. Subfraction H2 (100 mg) was subjected to semipreparative HPLC [F5, isocratic MeCN−H_2O (45:55), flow rate: 4 mL/min], yielding compounds **1** (2 mg, t_R = 8 min), **15** (25 mg, t_R = 9 min), and **2** (5 mg, t_R = 10 min). Subfraction H3 (450 mg) was subjected to semipreparative HPLC [F5, isocratic MeCN−H_2O (45:55), flow rate: 4 mL/min] to give compounds **16** (25 mg, t_R = 11 min) and **3** (5 mg, t_R = 12 min). Subfraction H5 (170 mg) was further purified by semipreparative HPLC [F5, isocratic MeCN−H_2O (47.5:52.5), flow rate: 4 mL/min] to give compounds **17** (2 mg, t_R = 9 min), **19** (3 mg, t_R = 10 min), **18** (8 mg, t_R = 11 min), and **4** (3 mg, t_R = 12 min). Compound **5** (5 mg, t_R = 11 min) was obtained from subfraction H6 by semipreparative HPLC [F5, isocratic MeCN−H_2O (1:1), flow rate: 4 mL/min].

*Trichorzin NPDG A (**1**):* colorless solid; $[\alpha]_D^{25}$ +14 (*c* 0.1, MeOH); ECD (MeOH, *c* 0.1) λ_{max} ($\Delta\varepsilon$) 208 (−157), 225 (−94.1); ^{1}H NMR (500 MHz, pyridine-d_5) and ^{13}C NMR (100 MHz, pyridine-d_5), see Table S3; HRESIMS *m*/*z* 852.5261 $[M + 2H]^{2+}$ (calcd for $C_{79}H_{140}N_{20}O_{21}$, 852.5245; mass error −1.9 ppm).

*Trichorzin NPDG B (**2**):* colorless solid; $[\alpha]_D^{25}$ −6 (*c* 0.1, MeOH); ECD (MeOH, *c* 0.1) λ_{max} ($\Delta\varepsilon$) 208 (−301), 225 (−175); ^{1}H NMR (500 MHz, pyridine-d_5) and ^{13}C NMR (100 MHz, pyridine-d_5), see Table S4; HRESIMS *m*/*z* 853.0184 $[M + 2H]^{2+}$ (calcd for $C_{79}H_{139}N_{19}O_{22}$, 853.0166; mass error −2.1 ppm).

*Trichorzin NPDG C (**3**):* colorless solid; $[\alpha]_D^{25}$ +10 (*c* 0.1, MeOH); ECD (MeOH, *c* 0.1) λ_{max} ($\Delta\varepsilon$) 208 (−326), 225 (−202); ^{1}H NMR (500 MHz, pyridine-d_5) and ^{13}C NMR (100 MHz, pyridine-d_5), see Table S5; HRESIMS *m*/*z* 866.5419 $[M + 2H]^{2+}$ (calcd for $C_{81}H_{144}N_{20}O_{21}$, 866.5402; mass error −2.0 ppm).

*Trichorzin NPDG D (**4**):* colorless solid; $[\alpha]_D^{25}$ +12 (*c* 0.1, MeOH); ECD (MeOH, *c* 0.1) λ_{max} ($\Delta\varepsilon$) 208 (−332), 225 (−200); ^{1}H NMR (500 MHz, pyridine-d_5) and ^{13}C NMR (100 MHz, pyridine-d_5), see Table S6; HRESIMS *m*/*z* 873.5493 $[M + 2H]^{2+}$ (calcd for $C_{82}H_{146}N_{20}O_{21}$, 873.5480; mass error −1.5 ppm).

*Trichorzin NPDG E (**5**):* colorless solid; $[\alpha]_D^{25}$ +4 (*c* 0.1, MeOH); ECD (MeOH, *c* 0.1) λ_{max} ($\Delta\varepsilon$) 208 (−249), 225 (−147); ^{1}H NMR (500 MHz, pyridine-d_5) and ^{13}C NMR (100 MHz, pyridine-d_5), see Table S7; HRESIMS *m*/*z* 880.5585 $[M + 2H]^{2+}$ (calcd for $C_{83}H_{148}N_{20}O_{21}$, 880.5558; mass error −3.1 ppm).

*Harzianin NPDG A (**6**):* colorless solid; $[\alpha]_D^{25}$ +12 (*c* 0.1, MeOH); ECD (MeOH, *c* 0.1) λ_{max} ($\Delta\varepsilon$) 205 (−163), 230 (−17.5); ^{1}H NMR (500 MHz, pyridine-d_5) and ^{13}C NMR (100 MHz, pyridine-d_5), see Table S8; HRESIMS *m*/*z* 1438.8705 $[M + Na]^+$ (calcd for $C_{68}H_{117}N_{15}NaO_{17}$, 1438.8644; mass error −4.2 ppm).

*Harzianin NPDG B (**7**):* colorless solid; $[\alpha]_D^{25}$ −4 (*c* 0.1, MeOH); ECD (MeOH, *c* 0.1) λ_{max} ($\Delta\varepsilon$) 205 (−211), 230 (−19.9); ^{1}H NMR (500 MHz, pyridine-d_5) and ^{13}C NMR (100 MHz, pyridine-d_5), see

https://dx.doi.org/10.1021/acs.jnatprod.0c01370
J. Nat. Prod. 2021, 84, 503−517

Table S9; HRESIMS *m/z* 715.9541 $[M + 2H]^{2+}$ (calcd for $C_{69}H_{121}N_{15}O_{17}$, 715.9527; mass error −2.0 ppm).

*Harzianin NPDG C (**8**):* colorless solid; $[\alpha]_D^{25}$ +30 (*c* 0.1, MeOH); ECD (MeOH, *c* 0.1) λ_{max} ($\Delta\varepsilon$) 205 (−184), 230 (−21.2); ^{1}H NMR (500 MHz, pyridine-d_5) and ^{13}C NMR (100 MHz, pyridine-d_5), see Table S10; HRESIMS *m/z* 715.9541 $[M + 2H]^{2+}$ (calcd for $C_{69}H_{121}N_{15}O_{17}$, 715.9527; mass error −2.0 ppm).

*Harzianin NPDG D (**9**):* colorless solid; $[\alpha]_D^{25}$ +36 (*c* 0.1, MeOH); ECD (MeOH, *c* 0.1) λ_{max} ($\Delta\varepsilon$) 205 (−175), 230 (−19.5); ^{1}H NMR (500 MHz, pyridine-d_5) and ^{13}C NMR (100 MHz, pyridine-d_5), see Table S11; HRESIMS *m/z* 722.9621 $[M + 2H]^{2+}$ (calcd for $C_{70}H_{123}N_{15}O_{17}$, 722.9605; mass error −2.2 ppm).

*Harzianin NPDG E (**10**):* colorless solid; $[\alpha]_D^{25}$ −6 (*c* 0.1, MeOH); ECD (MeOH, *c* 0.1) λ_{max} ($\Delta\varepsilon$) 205 (−196), 230 (−13.4); ^{1}H NMR (500 MHz, pyridine-d_5) and ^{13}C NMR (100 MHz, pyridine-d_5), see Table S12; HRESIMS *m/z* 707.9569 $[M + 2H]^{2+}$ (calcd for $C_{69}H_{121}N_{15}O_{16}$, 707.9552; mass error −2.4 ppm).

*Harzianin NPDG F (**11**):* colorless solid; $[\alpha]_D^{25}$ +40 (*c* 0.1, MeOH); ECD (MeOH, *c* 0.1) λ_{max} ($\Delta\varepsilon$) 205 (−119), 230 (−8.5); ^{1}H NMR (500 MHz, pyridine-d_5) and ^{13}C NMR (100 MHz, pyridine-d_5), see Table S13; HRESIMS *m/z* 714.9647 $[M + 2H]^{2+}$ (calcd for $C_{70}H_{123}N_{15}O_{16}$, 714.9631; mass error −2.2 ppm).

*Harzianin NPDG G (**12**):* colorless solid; $[\alpha]_D^{25}$ +38 (*c* 0.1, MeOH); ECD (MeOH, *c* 0.1) λ_{max} ($\Delta\varepsilon$) 205 (−149), 230 (−14.2); ^{1}H NMR (500 MHz, pyridine-d_5) and ^{13}C NMR (100 MHz, pyridine-d_5), see Table S14; HRESIMS *m/z* 714.9644 $[M + 2H]^{2+}$ (calcd for $C_{70}H_{123}N_{15}O_{16}$, 714.9631; mass error −1.8 ppm).

*Harzianin NPDG H (**13**):* colorless solid; $[\alpha]_D^{25}$ +6 (*c* 0.1, MeOH); ECD (MeOH, *c* 0.1) λ_{max} ($\Delta\varepsilon$) 205 (−147), 225 (−9.4); ^{1}H NMR (500 MHz, pyridine-d_5) and ^{13}C NMR (100 MHz, pyridine-d_5), see Table S15; HRESIMS *m/z* 721.9717 $[M + 2H]^{2+}$ (calcd for $C_{71}H_{125}N_{15}O_{16}$, 721.9709; mass error −1.1 ppm).

*Harzianin NPDG I (**14**):* colorless solid; $[\alpha]_D^{25}$ +12 (*c* 0.1, MeOH); ECD (MeOH, *c* 0.1) λ_{max} ($\Delta\varepsilon$) 207 (−36.8), 230 (−4.6); ^{1}H NMR (500 MHz, pyridine-d_5) and ^{13}C NMR (100 MHz, pyridine-d_5), see Table S16; HRESIMS *m/z* 1211.7720 $[M + Na]^+$ (calcd for $C_{59}H_{104}N_{12}NaO_{13}$, 1211.7738; mass error 1.5 ppm).

Extraction and Isolation of *H. pachybasioides*. Fungal biomass was extracted with 2 L of EtOAc (×3) at room temperature, the organic solvent layers were recovered, and the solvent was removed under vacuum. The EtOAc-soluble material was combined for further processing (21 g; fraction A). Fraction A was subjected to silica gel vacuum column chromatography with elution performed using dichloromethane (fraction B), dichloromethane−MeOH (10:1) (fraction C), and MeOH (fraction D). Fraction D (5 g) was subjected to preparative HPLC (C_{18}, isocratic 85% MeOH−H_2O, flow rate: 10 mL/min) to afford nine fractions (fractions E−M). Fraction E (25 mg) was subjected to semipreparative HPLC [biphenyl, isocratic MeCN−H_2O (1:1), flow rate: 4 mL/min] to give compounds **29** (2 mg, t_R = 9 min) and **28** (6 mg, t_R = 10 min). Fraction F (20 mg) was subjected to semipreparative HPLC [biphenyl, isocratic MeCN−H_2O (1:1), flow rate: 4 mL/min], yielding compounds **31** (2 mg, t_R = 8 min), **32** (5 mg, t_R = 9 min), and **30** (25 mg, t_R = 11 min). Fraction H (300 mg) was separated into four subfractions (H1−4) by preparative HPLC (C_{18}, gradient elution with 80−100% MeOH in H_2O over 20 min, flow rate: 10 mL/min). Subfraction H1 (130 mg) was subjected to semipreparative HPLC [biphenyl, isocratic MeCN−H_2O (1:1), flow rate: 4 mL/min] to give compounds **44** (15 mg, t_R = 9 min) and **34** (37 mg, t_R = 10 min). Subfraction H2 (50 mg) was subjected to semipreparative HPLC [biphenyl, isocratic MeCN−H_2O (47.5:52.5), flow rate: 4 mL/min] to obtain compounds **48** (6 mg, t_R = 10 min), **47** (6 mg, t_R = 11 min), and **33** (3 mg, t_R = 16 min). Fraction I was fractionated into four subfractions (I1−4) by preparative HPLC (C_{18}, gradient elution with MeOH in H_2O over 15 min, flow rate: 10 mL/min). Compound **49** (4 mg, t_R = 11 min) was purified from subfraction I1 (15 mg) by semipreparative HPLC [F5, MeCN−H_2O (45:55), flow rate: 4 mL/min]. Subfraction I3 (65 mg) was further subjected to semipreparative HPLC [biphenyl, isocratic MeCN−H_2O (1:1), flow rate: 4 mL/min], yielding compounds **35** (2 mg, t_R = 11 min), **45** (2 mg, t_R = 12 min), and **36** (3 mg, t_R = 13 min). Fraction J (90 mg) was further purified by semipreparative HPLC [biphenyl, isocratic MeCN−H_2O (45:55), flow rate: 4 mL/min] to give compounds **50** (25 mg, t_R = 9 min) and **51** (2 mg, t_R = 10 min). Compound **52** (35 mg, t_R = 10 min) was purified from fraction L (60 mg) by semipreparative HPLC [F5, isocratic MeCN−H_2O (47.5:52.5), flow rate: 4 mL/min]. Fraction M (500 mg) was fractionated into five subfractions using HP20ss gel vacuum column chromatography: subfractions M1 (30% MeOH), M2 (50% MeOH), M3 (70% MeOH), M4 (90% MeOH), and M5 (100% MeOH). Fraction M4 (180 mg) was separated into five subfractions (M4-1−M4-5) by preparative HPLC (C_{18}, gradient elution with 85−100% MeOH in H_2O over 15 min, flow rate: 10 mL/min). Subfraction M4-3 (20 mg) was further subjected to semipreparative HPLC [F5, isocratic MeCN−H_2O (1:1), flow rate: 4 mL/min] to yield compounds **38** (1.5 mg, t_R = 11 min), **39** (3 mg, t_R = 12 min), and **43** (2 mg, t_R = 13 min). Subfraction M4-4 (30 mg) was subjected to semipreparative HPLC [F5, isocratic MeCN−H_2O (52.5:47.5), flow rate: 4 mL/min] to give compounds **37** (3 mg, t_R = 7 min), **42** (4 mg, t_R = 9 min), and **46** (6 mg, t_R = 11 min). Compounds **40** (6 mg, t_R = 8 min) and **41** (7 mg, t_R = 9 min) were obtained from subfraction M4-5 by semipreparative HPLC [biphenyl, isocratic MeCN−H_2O (1:1), flow rate: 4 mL/min).

*Hypocrin NPDG A (**28**):* colorless solid; $[\alpha]_D^{25}$ −14 (*c* 0.1, MeOH); ECD (MeOH, *c* 0.1) λ_{max} ($\Delta\varepsilon$) 215 (+21.5); ^{1}H NMR (500 MHz, pyridine-d_5) and ^{13}C NMR (100 MHz, pyridine-d_5), see Table S17; HRESIMS *m/z* 740.5278 $[M + H]^+$ (calcd for $C_{37}H_{70}N_7O_8$, 740.5280; mass error 0.3 ppm).

*Hypocrin NPDG B (**29**):* colorless solid; $[\alpha]_D^{25}$ +6 (*c* 0.1, MeOH); ECD (MeOH, *c* 0.1) λ_{max} ($\Delta\varepsilon$) 215 (+5.6); ^{1}H NMR (500 MHz, pyridine-d_5) and ^{13}C NMR (100 MHz, pyridine-d_5), see Table S18; HRESIMS *m/z* 740.5292 $[M + H]^+$ (calcd for $C_{37}H_{70}N_7O_8$, 740.5280; mass error −1.6 ppm).

*Hypocrin NPDG C (**30**):* colorless solid; $[\alpha]_D^{25}$ −4 (*c* 0.1, MeOH); ECD (MeOH, *c* 0.1) λ_{max} ($\Delta\varepsilon$) 215 (+8.0);^{1}H NMR (500 MHz, pyridine-d_5) and ^{13}C NMR (100 MHz, pyridine-d_5), see Table S19; HRESIMS *m/z* 754.5453 $[M + H]^+$ (calcd for $C_{38}H_{72}N_7O_8$, 754.5437; mass error −2.1 ppm).

*Hypocrin NPDG D (**31**):* colorless solid; $[\alpha]_D^{25}$ −8 (*c* 0.1, MeOH); ECD (MeOH, *c* 0.1) λ_{max} ($\Delta\varepsilon$) 206 (−44.6), 223 (−24.7); ^{1}H NMR (500 MHz, pyridine-d_5) and ^{13}C NMR (100 MHz, pyridine-d_5), see Table S20; HRESIMS *m/z* 1024.6771 $[M + H]^+$ (calcd for $C_{49}H_{90}N_{11}O_{12}$, 1024.6765; mass error −0.6 ppm).

*Hypocrin NPDG E (**32**):* colorless solid; $[\alpha]_D^{25}$ −8 (*c* 0.1, MeOH); ECD (MeOH, *c* 0.1) λ_{max} ($\Delta\varepsilon$) 205 (−60.4), 222 (−26.5); ^{1}H NMR (500 MHz, pyridine-d_5) and ^{13}C NMR (100 MHz, pyridine-d_5), see Table S21; HRESIMS *m/z* 1038.6919 $[M + H]^+$ (calcd for $C_{50}H_{92}N_{11}O_{12}$, 1038.6921; mass error 0.2 ppm).

*Hypocrin NPDG F (**33**):* colorless solid; $[\alpha]_D^{25}$ −22 (*c* 0.1, MeOH); ECD (MeOH, *c* 0.1) λ_{max} ($\Delta\varepsilon$) 205 (−76.3), 223 (−28.4); ^{1}H NMR (500 MHz, pyridine-d_5) and ^{13}C NMR (100 MHz, pyridine-d_5), see Table S22; HRESIMS *m/z* 1052.7061 $[M + H]^+$ (calcd for $C_{51}H_{94}N_{11}O_{12}$, 1052.7078; mass error 1.6 ppm).

*Hypocrin NPDG G (**34**):* colorless solid; $[\alpha]_D^{25}$ −24 (*c* 0.1, MeOH); ECD (MeOH, *c* 0.1) λ_{max} ($\Delta\varepsilon$) 205 (−89.6), 222 (−36.0); ^{1}H NMR (500 MHz, pyridine-d_5) and ^{13}C NMR (100 MHz, pyridine-d_5), see Table S23; HRESIMS *m/z* 1052.7062 $[M + H]^+$ (calcd for $C_{51}H_{94}N_{11}O_{12}$, 1052.7078; mass error 1.5 ppm).

*Hypocrin NPDG H (**35**):* colorless solid; $[\alpha]_D^{25}$ −10 (*c* 0.1, MeOH); ECD (MeOH, *c* 0.1) λ_{max} ($\Delta\varepsilon$) 206 (−103), 223 (−48.8); ^{1}H NMR (500 MHz, pyridine-d_5) and ^{13}C NMR (100 MHz, pyridine-d_5), see Table S24; HRESIMS *m/z* 1052.7076 $[M + H]^+$ (calcd for $C_{51}H_{94}N_{11}O_{12}$, 1052.7078; mass error 0.2 ppm).

*Hypocrin NPDG I (**36**):* colorless solid; $[\alpha]_D^{25}$ +8 (*c* 0.1, MeOH); ECD (MeOH, *c* 0.1) λ_{max} ($\Delta\varepsilon$) 206 (−42.3), 223 (−65.7); ^{1}H NMR (500 MHz, pyridine-d_5) and ^{13}C NMR (100 MHz, pyridine-d_5), see Table S25; HRESIMS *m/z* 1088.7073 $[M + Na]^+$ (calcd for $C_{52}H_{95}N_{11}NaO_{12}$, 1088.7054; mass error −1.7 ppm).

*Hypocrin NPDG J (**37**):* colorless solid; $[\alpha]_D^{25}$ +6 (*c* 0.1, MeOH); ECD (MeOH, *c* 0.1) λ_{max} ($\Delta\varepsilon$) 206 (−94.6), 222 (−65.7); ^{1}H NMR

https://dx.doi.org/10.1021/acs.jnatprod.0c01370
J. Nat. Prod. 2021, 84, 503−517

(500 MHz, pyridine-d_5) and ^{13}C NMR (100 MHz, pyridine-d_5), see Table S26; HRESIMS m/z 1358.8427 $[M + Na]^+$ (calcd for $C_{63}H_{113}N_{15}NaO_{16}$, 1358.8382; mass error −3.3 ppm).

*Hypocrin NPDG K (**38**):* colorless solid; $[\alpha]_D^{25}$ +2 (c 0.1, MeOH); ECD (MeOH, c 0.1) λ_{max} ($\Delta\varepsilon$) 206 (−71.9), 222 (−49.7); ^{1}H NMR (500 MHz, pyridine-d_5) and ^{13}C NMR (100 MHz, pyridine-d_5), see Table S27; HRESIMS m/z 1372.8540 $[M + Na]^+$ (calcd for $C_{64}H_{115}N_{15}NaO_{16}$, 1372.8538; mass error −0.1 ppm).

*Hypocrin NPDG L (**39**):* colorless solid; $[\alpha]_D^{25}$ −12 (c 0.1, MeOH); ECD (MeOH, c 0.1) λ_{max} ($\Delta\varepsilon$) 206 (−99.9), 222 (−64.8); ^{1}H NMR (500 MHz, pyridine-d_5) and ^{13}C NMR (100 MHz, pyridine-d_5), see Table S28; HRESIMS m/z 1350.8716 $[M + H]^+$ (calcd for $C_{64}H_{116}N_{15}O_{16}$, 1350.8719; mass error 0.2 ppm).

*Hypocrin NPDG M (**40**):* colorless solid; $[\alpha]_D^{25}$ +6 (c 0.1, MeOH); ECD (MeOH, c 0.1) λ_{max} ($\Delta\varepsilon$) 206 (−188), 222 (−116); ^{1}H NMR (500 MHz, pyridine-d_5) and ^{13}C NMR (100 MHz, pyridine-d_5), see Table S29; HRESIMS m/z 1372.8555 $[M + Na]^+$ (calcd for $C_{64}H_{115}N_{15}NaO_{16}$, 1372.8538; mass error −1.2 ppm).

*Hypocrin NPDG N (**41**):* colorless solid; $[\alpha]_D^{25}$ −4 (c 0.1, MeOH); ECD (MeOH, c 0.1) λ_{max} ($\Delta\varepsilon$) 206 (−152), 222 (−89.7); ^{1}H NMR (500 MHz, pyridine-d_5) and ^{13}C NMR (100 MHz, pyridine-d_5), see Table S30; HRESIMS m/z 1386.8720 $[M + Na]^+$ (calcd for $C_{65}H_{117}N_{15}NaO_{16}$, 1386.8695; mass error −1.8 ppm).

*Hypocrin NPDG O (**42**):* colorless solid; $[\alpha]_D^{25}$ −12 (c 0.1, MeOH); ECD (MeOH, c 0.1) λ_{max} ($\Delta\varepsilon$) 206 (−93.9), 222 (−53.4); ^{1}H NMR (500 MHz, pyridine-d_5) and ^{13}C NMR (100 MHz, pyridine-d_5), see Table S31; HRESIMS m/z 1386.8722 $[M + Na]^+$ (calcd for $C_{65}H_{117}N_{15}NaO_{16}$, 1386.8695; mass error −1.9 ppm).

*Hypocrin NPDG P (**43**):* colorless solid; $[\alpha]_D^{25}$ −10 (c 0.1, MeOH); ECD (MeOH, c 0.1) λ_{max} ($\Delta\varepsilon$) 206 (−46.0), 222 (−28.3); ^{1}H NMR (500 MHz, pyridine-d_5) and ^{13}C NMR (100 MHz, pyridine-d_5), see Table S32; HRESIMS m/z 1386.8685 $[M + Na]^+$ (calcd for $C_{65}H_{117}N_{15}NaO_{16}$, 1386.8695; mass error 0.7 ppm).

Preparation of Amino Acid Standards and Absolute Configuration Analysis of Amino Acid Residues. Peptaibols (0.3 mg) were hydrolyzed in 300 μL of 6 N HCl at 110 °C overnight. After cooling to room temperature, the hydrolysate neutralized by 2 N NaOH was evaporated to dryness and the remaining residue dissolved in 100 μL of water and 1 M $NaHCO_3$ (30 μL). A solution of *N*-α-(2,4-dinitro-5-fluorophenyl)-L-alaninamide (L-FDAA, Marfey's reagent, Sigma, 100 μL, 1% in acetone) was added to each reaction vial. The reaction mixture was heated to 45 °C for 1 h, quenched by adding 1 N HCl (30 μL), and mixed with CH_3CN (1 mL). Samples consisting of 5 μL of the FDAA derivatives were taken for LC/MS analysis (Kinetex C_{18}, 2.6 μm, 100 Å, 75 × 3.0 mm, flow rate: 0.4 mL/min), which was performed at room temperature. Aqueous CH_3CN containing 0.1% formic acid was used as the mobile phase in gradient mode (10−50% CH_3CN in H_2O over 30 min). The D- and L-amino acid authentic standards were prepared similarly. The following retention times (min) were observed for the L-FDAA derivatives of the standards: 11.1 (L-Ser), 11.7 (D-Ser), 12.1 (L-Asp), 13.2 (D-Asp), 13.5 (L-Glu), 14.6 (D-Glu), 14.6 (L-Ala), 16.7 (D-Ala), 15.2 (L-Pro), 16.1 (D-Pro), 19.0 (L-Val), 21.8 (D-Val), 19.2 (L-Iva), 20.3 (D-Iva), 21.0 (L-Leuol), 24.2 (D-Leuol), 21.6 (L-Ile), 24.2 (D-Ile), 21.6 (L-*allo*-Ile), 24.2 (D-*allo*-Ile), 22.0 (L-Leu), and 24.5 (D-Leu).

Absolute Configuration Analysis of Isoleucine Residues. Hydrolysates of the metabolites were prepared as described for the Marfey's analysis (*vide supra*), and the residue was dissolved in H_2O (100 μL). Aliquots consisting of 200 μL of 5% trimethylamine in acetone and 200 μL of 1% GITC solution in acetone were added to the hydrolysate. Reaction vials were maintained at room temperature (~25 °C) for 15 min before being quenched by adding 200 μL of 5% acetic acid. For LC/MS analyses, 5 μL aliquots of the GITC derivatives were prepared and tested at room temperature (Kinetex C_{18}, 2.6 μm, 100 Å, 75 × 3.0 mm, flow rate: 0.4 mL/min, 10−30% CH_3CN−H_2O with 0.1% formic acid for 0−50 min). Standards consisting of authentic L-isoleucine and L-*allo*-isoleucine were prepared in the same fashion. The following retention times were observed for the GITC derivatives of the standards: t_R (min) 48.5 (L-*allo*-Ile) and 49.0 (L-Ile).

X-ray Crystallographic Analysis of Compound 40. Crystals of compound **40** were obtained from MeOH−water (5:1). A colorless, block-shaped crystal of dimensions 0.060 × 0.104 × 0.186 mm was selected for structural analysis. Intensity data were collected using a D8 Quest κ-geometry diffractometer with a Bruker Photon II cmos area detector and an Incoatec Iμs microfocus Mo Kα source (λ = 0.710 73 Å). The sample was cooled to 100(2) K. Cell parameters were determined from a least-squares fit of 9954 peaks in the range $2.19° < \theta < 23.11°$. A total of 50 593 data points were measured in the range $2.090° < \theta < 19.027°$ using φ and ω oscillation frames. The data were corrected for absorption by the empirical method, giving minimum and maximum transmission factors of 0.5817 and 0.7453. The data were merged to form a set of 23 614 independent data with R(int) = 0.0917 and a coverage of 99.4%. Crystallographic data for **40** have been deposited at the Cambridge Crystallographic Data Centre (deposition number: CCDC 1967991). Copies of these data can be obtained free of charge from the CCDC via www.ccdc.cam.ac.uk.

Parasite Culture Conditions. The *P. falciparum* culture was maintained following a modified Trager and Jensen protocol.[48] The multi-drug-resistant *P. falciparum* line Dd2 was grown in RPMI 1640 supplemented with 25 mM HEPES pH 7.4, 26 mM $NaHCO_3$, 2% dextrose, 15 mg/L hypoxanthine, 25 mg/L gentamicin, and 0.5% Albumax II in human A+ erythrocytes. Cultures were maintained at 4% hematocrit at 37 °C with 5% CO_2.

Phenotypic Screen for Antiplasmodial Activity. Antiplasmodial EC_{50} results were determined using a fluorescence-based SYBR Green I assay performed using asynchronous cultures.[49] For screening, parasites were diluted to 1% parasitemia and 2% hematocrit, then incubated with serial dilutions of compounds in microtiter plates for 72 h at standard growth conditions. Plates were subsequently frozen at −80 °C to facilitate lysis. After thawing, plates were incubated with 1× SYBR Green I in lysis buffer (20 mM Tris-HCl, 0.08% saponin, 5 mM EDTA, 0.8% Triton X-100) for 45 min at room temperature. Fluorescence was measured at an excitation wavelength of 485 nm and emission wavelength of 530 nm in a Synergy Neo2 multimode reader (BioTek, Winsooki, VT, USA). Relative fluorescence units (RFUs) were normalized based on chloroquine-treated and no treatment controls. Serial dilutions of compounds were prepared in RPMI with final assay conditions of ≤0.2% DMSO.

Human Cell Cytotoxicity Assay. Mammalian cell cytotoxicity was assessed in HepG2 human hepatocytes using an MTS (3-(4,5-dimethylthiazol-2-yl)-5-(3-carboxymethoxyphenyl)-2-(4-sulfophenyl)-2*H*-tetrazolium)-based cytotoxicity assay. For cytotoxicity testing, ~2250 cells were seeded into each well of a 384-well microtiter plate, and the cells were incubated for 24 h. Serial dilutions of the compounds were added in triplicate starting at 25 μM (final concentration). This maximum concentration was chosen to maintain a consistently high concentration without sacrificing compound solubility, while also keeping DMSO concentration below toxic levels. Cells were further incubated for an additional 48 h at 37 °C in an atmosphere containing 5% CO_2. Zero percent growth control wells were incubated with 5% Triton X-100 for 5 min prior to MTS addition. Following the addition of MTS to all wells, the plates were incubated for an additional 4 h under the same environmental conditions before taking absorbance measurements. Absorbance values were recorded at 490 nm using a Synergy Neo2 multimode reader (BioTek), and values were normalized based on Triton X-100-lysed and no treatment controls.

■ ASSOCIATED CONTENT

Supporting Information

The Supporting Information is available free of charge at https://pubs.acs.org/doi/10.1021/acs.jnatprod.0c01370.

1D NMR, 2D NMR, HRESIMS, MS/MS fragment analysis, and ECD spectrum for new peptaibols **1**−**14** and **28**−**43** (PDF)

https://dx.doi.org/10.1021/acs.jnatprod.0c01370
J. Nat. Prod. 2021, 84, 503−517

Crystallographic information file for compound **40** (CIF)

AUTHOR INFORMATION

Corresponding Authors

Robert H. Cichewicz − *Natural Products Discovery Group, Institute for Natural Products Applications and Research Technologies, Department of Chemistry and Biochemistry, Stephenson Life Sciences Research Center, University of Oklahoma, Norman, Oklahoma 73019, United States;* orcid.org/0000-0003-0744-4117; Email: rhcichewicz@ou.edu

Debopam Chakrabarti − *Division of Molecular Microbiology, Burnett School of Biomedical Sciences, University of Central Florida, Orlando, Florida 32826, United States;* Email: Debopam.Chakrabarti@ucf.edu

Authors

Jin Woo Lee − *Natural Products Discovery Group, Institute for Natural Products Applications and Research Technologies, Department of Chemistry and Biochemistry, Stephenson Life Sciences Research Center, University of Oklahoma, Norman, Oklahoma 73019, United States*

Jennifer E. Collins − *Division of Molecular Microbiology, Burnett School of Biomedical Sciences, University of Central Florida, Orlando, Florida 32826, United States;* orcid.org/0000-0002-1195-4630

Karen L. Wendt − *Natural Products Discovery Group, Institute for Natural Products Applications and Research Technologies, Department of Chemistry and Biochemistry, Stephenson Life Sciences Research Center, University of Oklahoma, Norman, Oklahoma 73019, United States*

Complete contact information is available at: https://pubs.acs.org/10.1021/acs.jnatprod.0c01370

Author Contributions

[§]J. W. Lee and J. E. Collins contributed equally to this work.

Notes

The authors declare no competing financial interest.

ACKNOWLEDGMENTS

Support for this project was provided by NIH grants R21AI143052 and R01AI154777 to D.C. and R.H.C. An LC-MS instrument used for this project was provided in part by a Challenge Grant from the Office of the Vice President for Research, University of Oklahoma, Norman Campus, and an award through the Shimadzu Equipment Grant Program (R.H.C.). A grant from the NSF (CHE-0130835) was used for the purchase of the X-ray diffractometer. We thank Dr. D. R. Powell for his technical assistance with the X-ray diffraction analysis. We are grateful for the gift of soil samples provided by citizen scientists J. Smith and T. Elliot that were used to obtain fungi described in this report.

REFERENCES

(1) World Health Organization. *World Malaria Report 2020*; Geneva, Switzerland, 2020.

(2) Adam, I.; Ibrahim, Y.; Gasim, G. I. *Malar. J.* **2018**, *17*, 110.

(3) World Health Organization. *Artemisinin Resistance and Artemisinin-Based Combination Therapy Efficacy*; Geneva, Switzerland, 2019.

(4) Straimer, J.; Gnadig, N. F.; Witkowski, B.; Amaratunga, C.; Duru, V.; Ramadani, A. P.; Dacheux, M.; Khim, N.; Zhang, L.; Lam, S.; Gregory, P. D.; Urnov, F. D.; Mercereau-Puijalon, O.; Benoit-Vical, F.; Fairhurst, R. M.; Menard, D.; Fidock, D. A. *Science* **2015**, *347*, 428−31.

(5) Imwong, M.; Dhorda, M.; Tun, K. M.; Thu, A. M.; Phyo, A. P.; Proux, S.; Suwannasin, K.; Kunasol, C.; Srisutham, S.; Duanguppama, J. *Lancet Infect. Dis.* **2020**, *20*, 1470−80.

(6) Lacerda, A. F.; Pelegrini, P. B.; de Oliveira, D. M.; Vasconcelos, É. A.; Grossi-de-Sá, M. F. *Front. Microbiol.* **2016**, *7*, 91.

(7) Boman, H.; Wade, D.; Boman, I.; Wåhlin, B.; Merrifield, R. *FEBS Lett.* **1989**, *259*, 103−6.

(8) Gwadz, R.; Kaslow, D.; Lee, J.-Y.; Maloy, W.; Zasloff, M.; Miller, L. *Infect. Immun.* **1989**, *57*, 2628−33.

(9) Carballar-Lejarazú, R.; Rodriguez, M.; de la Cruz Hernandez-Hernandez, F.; Ramos-Castaneda, J.; Possani, L.; Zurita-Ortega, M.; Reynaud-Garza, E.; Hernandez-Rivas, R.; Loukeris, T.; Lycett, G. *Cell. Mol. Life Sci.* **2008**, *65*, 3081−92.

(10) Gao, B.; Xu, J.; del Carmen Rodriguez, M.; Lanz-Mendoza, H.; Hernández-Rivas, R.; Du, W.; Zhu, S. *Biochimie* **2010**, *92*, 350−9.

(11) Vizioli, J.; Bulet, P.; Hoffmann, J. A.; Kafatos, F. C.; Müller, H.-M.; Dimopoulos, G. *Proc. Natl. Acad. Sci. U. S. A.* **2001**, *98*, 12630−5.

(12) Linington, R. G.; Clark, B. R.; Trimble, E. E.; Almanza, A.; Urena, L.-D.; Kyle, D. E.; Gerwick, W. H. *J. Nat. Prod.* **2009**, *72*, 14−7.

(13) Zhao, L.; Kaiser, M.; Bode, H. B. *Org. Lett.* **2018**, *20*, 5116−20.

(14) Singh, S. B.; Zink, D. L.; Liesch, J. M.; Dombrowski, A. W.; Darkin-Rattray, S. J.; Schmatz, D. M.; Goetz, M. A. *Org. Lett.* **2001**, *3*, 2815−8.

(15) Hayashi, Y.; Fukasawa, W.; Hirose, T.; Iwatsuki, M.; Hokari, R.; Ishiyama, A.; Kanaida, M.; Nonaka, K.; Také, A.; Otoguro, K. *Org. Lett.* **2019**, *21*, 2180−4.

(16) Nagaraj, G.; Uma, M.; Shivayogi, M.; Balaram, H. *Antimicrob. Agents Chemother.* **2001**, *45*, 145−9.

(17) Du, L.; Robles, A. J.; King, J. B.; Powell, D. R.; Miller, A. N.; Mooberry, S. L.; Cichewicz, R. H. *Angew. Chem., Int. Ed.* **2014**, *53*, 804−9.

(18) Jaworski, A.; Kirschbaum, J.; Brückner, H. *J. Pept. Sci.* **1999**, *5*, 341−51.

(19) Przybylski, M.; Dietrich, I.; Manz, I.; Brückner, H. *Biomed. Mass Spectrom.* **1984**, *11*, 569−82.

(20) Iida, A.; Sanekata, M.; Wada, S.-i.; Fujita, T.; Tanaka, H.; Enoki, A.; Fuse, G.; Kanai, M.; Asami, K. *Chem. Pharm. Bull.* **1995**, *43*, 392−7.

(21) Oh, S.-U.; Yun, B.-S.; Lee, S.-J.; Kim, J.-H.; Yoo, I.-D. *J. Antibiot.* **2002**, *55*, 557−64.

(22) Jaworski, A.; Brückner, H. *J. Chromatogr. A* **1999**, *862*, 179−89.

(23) Jiao, W.-H.; Khalil, Z.; Dewapriya, P.; Salim, A. A.; Lin, H.-W.; Capon, R. J. *J. Nat. Prod.* **2018**, *81*, 976−84.

(24) Goulard, C.; Hlimi, S.; Rebuffat, S.; Bodo, B. *J. Antibiot.* **1995**, *48*, 1248−53.

(25) Hlimi, S.; Rebuffat, S.; Goulard, C.; Duchamp, S.; Bodo, B. *J. Antibiot.* **1995**, *48*, 1254−61.

(26) Fujii, K.; Ikai, Y.; Mayumi, T.; Oka, H.; Suzuki, M.; Harada, K.-i. *Anal. Chem.* **1997**, *69*, 3346−52.

(27) Fujii, K.; Ikai, Y.; Oka, H.; Suzuki, M.; Harada, K.-i. *Anal. Chem.* **1997**, *69*, 5146−51.

(28) Liu, D.; Lin, H.; Proksch, P.; Tang, X.; Shao, Z.; Lin, W. *Org. Lett.* **2015**, *17*, 1220−3.

(29) De Zotti, M.; Damato, F.; Formaggio, F.; Crisma, M.; Schievano, E.; Mammi, S.; Kaptein, B.; Broxterman, Q. B.; Felock, P. J.; Hazuda, D. J. *Chem. - Eur. J.* **2010**, *16*, 316−27.

(30) Grauer, A. A.; Cabrele, C.; Zabel, M.; König, B. *J. Org. Chem.* **2009**, *74*, 3718−26.

(31) Hess, S.; Gustafson, K. R.; Milanowski, D. J.; Alvira, E.; Lipton, M. A.; Pannell, L. K. *J. Chromatogr. A* **2004**, *1035*, 211−9.

(32) Rebuffat, S.; Goulard, C.; Bodo, B. *J. Chem. Soc., Perkin Trans. 1* **1995**, *14*, 1849−55.

(33) Augeven-Bour, I.; Rebuffat, S.; Auvin, C.; Goulard, C.; Prigent, Y.; Bodo, B. *J. Chem. Soc., Perkin Trans. 1* **1997**, *10*, 1587−94.

(34) Singh, V. P.; Yedukondalu, N.; Sharma, V.; Kushwaha, M.; Sharma, R.; Chaubey, A.; Kumar, A.; Singh, D.; Vishwakarma, R. A. *J. Nat. Prod.* **2018**, *81*, 219−26.
(35) Tsantrizos, Y. S.; Pischos, S.; Sauriol, F.; Widden, P. *Can. J. Chem.* **1996**, *74*, 165−72.
(36) Röhrich, C. R.; Iversen, A.; Jaklitsch, W. M.; Voglmayr, H.; Vilcinskas, A.; Nielsen, K. F.; Thrane, U.; Von Döhren, H.; Brückner, H.; Degenkolb, T. *Chem. Biodiversity* **2013**, *10*, 787−812.
(37) Degenkolb, T.; Gräfenhan, T.; Berg, A.; Nirenberg, H. I.; Gams, W.; Brückner, H. *Chem. Biodiversity* **2006**, *3*, 593−610.
(38) Longo, E.; Moretto, A.; Formaggio, F.; Toniolo, C. *Chirality* **2011**, *23*, 756−60.
(39) Adler, A. J.; Greenfield, N. J.; Fasman, G. D. *Methods Enzymol.* **1973**, *27*, 675−735.
(40) Du, L.; Risinger, A. L.; Mitchell, C. A.; You, J.; Stamps, B. W.; Pan, N.; King, J. B.; Bopassa, J. C.; Judge, S. I.; Yang, Z. *Proc. Natl. Acad. Sci. U. S. A.* **2017**, *114*, 8957−66.
(41) Auvin-Guette, C.; Rebuffat, S.; Vuidepot, I.; Massias, M.; Bodo, B. *J. Chem. Soc., Perkin Trans. 1* **1993**, *2*, 249−55.
(42) Auvin-Guette, C.; Rebuffat, S.; Prigent, Y.; Bodo, B. *J. Am. Chem. Soc.* **1992**, *114*, 2170−4.
(43) China, N.; Blond, A.; Goulard, C.; Bodo, B.; Rebuffat, S. *J. Pept. Sci.*; **2000**, *6*, 519.
(44) Fujita, T.; Iida, A.; Uesato, S.; Takaishi, Y.; Shingu, T.; Saito, M.; Morita, M. *J. Antibiot.* **1988**, *41*, 814−8.
(45) Huang, Q.; Tezuka, Y.; Kikuchi, T.; Nishi, A.; Tubaki, K.; Tanaka, K. *Chem. Pharm. Bull.* **1995**, *43*, 223−9.
(46) Iwatsuki, M.; Kinoshita, Y.; Niitsuma, M.; Hashida, J.; Mori, M.; Ishiyama, A.; Namatame, M.; Nishihara-Tsukashima, A.; Nonaka, K.; Masuma, R. *J. Antibiot.* **2010**, *63*, 331−3.
(47) Bandani, A.; Khambay, B. P. S.; Faull, J.; Newton, R.; Deadman, M.; Butt, T. *Mycol. Res.* **2000**, *104*, 537−44.
(48) Trager, W.; Jensen, J. B. *Science* **1976**, *193*, 673−5.
(49) Smilkstein, M.; Sriwilaijaroen, N.; Kelly, J. X.; Wilairat, P.; Riscoe, M. *Antimicrob. Agents Chemother.* **2004**, *48*, 1803−6.

https://dx.doi.org/10.1021/acs.jnatprod.0c01370
J. Nat. Prod. 2021, 84, 503−517